THE ASTROPHYSICAL JOURNAL, 412:127–145, 1993 July 20


# THE NATURE OF UNIDENTIFIED FAR-INFRARED POINT SOURCES

WILLIAM T. REACH,[1,2] CARL HEILES,[1] AND BON-CHUL KOO[1,3]
*Received 1992 November 23; accepted 1993 February 1*

## ABSTRACT

Sources discovered by the *Infrared Astronomical Satellite* with spectra that rise steeply from 60 to 100 $\mu$m are a mixed sample of external galaxies, condensations in the interstellar medium, and potentially unknown astronomical objects. Sources in regions of low total H I column density (as determined with the all-sky 21 cm line surveys), and with no nearby cataloged external galaxy, were observed for presence of 20 cm continuum emission (with the NRAO Very Large Array), enhanced 21 cm H I line emission (with the NAIC Arecibo 305 m), and molecular line emission (with the NRAO 12 m, HCRO 6 m, and FCRAO 14 m). Based on the CO detection rate, 70% of our sample are small interstellar molecular clouds. The remainder are mostly faint external galaxies. The dust column densities of the interstellar condensations were determined from the infrared flux, using a spherical-cloud model for the radiative transfer of the interstellar radiation field (ISRF). The CO column densities were determined using the large-velocity-gradient model for the excitation and radiative transfer of the rotational transitions. About half of the interstellar sources have normal dust-to-gas ratios and ISRF heating. Sources with excess infrared emission, compared to the molecular column density, are protostellar candidates. Sources in the Draco nebula are rich in CO but deficient in dust. The remaining interstellar sources, which have pressure some two orders of magnitude higher than the average interstellar pressure, may be accretion nebulae around stellar remnants.

*Subject headings:* dust, extinction — infrared: galaxies — infrared: interstellar: continuum — ISM: molecules

## 1. INTRODUCTION

The *Infrared Astronomical Satellite* (*IRAS*) in 1983 performed the first all-sky survey at wavelengths of 12, 25, 60, and 100 $\mu$m. A new class of astronomical object discovered by *IRAS* consists of the $\sim 10^4$ point sources detected only at 100 $\mu$m (or with barely detected 60 $\mu$m flux). Due to the similarity of the 60–100 $\mu$m spectra to that of the "infrared cirrus"—high-latitude interstellar atomic and molecular clouds—we refer to these sources as "cirrus point sources." Specifically, cirrus point sources are regions smaller than $\sim 5'$ with 100 $\mu$m brightness enhanced by more than a factor of 5 over the local background level. In this paper we describe the properties of a sample of cirrus point sources that are not associated with any known astronomical source. Included among the cirrus point sources are the objects that are relatively brightest at submillimeter wavelengths, if the *IRAS* spectra may be extrapolated as a blackbody or power law. With the rapid development of technology for detecting submillimeter radiation, cirrus point sources are candidates for future observation.

Many cirrus point sources can be associated with known astronomical objects. Galaxies have far-infrared spectra that peak just longward of 100 $\mu$m (Young et al. 1989), and the *IRAS* sensitivity to galaxian far-infrared radiation is comparable (for spiral galaxies) to that of optical surveys based on the Palomar Observatory Sky Survey. If the cirrus point sources were all galaxies, they would represent a sample of infrared-bright, and in some cases perhaps "ultraluminous" galaxies and quasars (Houck et al. 1985).

A likely hypothesis for the nature of cirrus point sources is that they are clumps in the interstellar medium. Many high-latitude interstellar clouds contain several cirrus point sources as well as infrared-bright regions that did not satisfy the *IRAS* point source selection criteria because they were partially resolved. Millimeter and radio spectral-line observations of clumps in high-latitude molecular clouds indicate they are regions of locally enhanced volume density (Turner, Rickard, & Xu 1989; Pound, Bania, & Wilson 1990). In the Galactic plane, bright cirrus point sources generally correspond to star-forming molecular clouds of order $10^3\ M_\odot$ (Casoli et al. 1986).

In this paper we attempt to determine the nature of those infrared cirrus point sources that are *not* associated with known astronomical objects. In order to maximize the probability that a source is not associated with an interstellar cloud, we exclude the Galactic plane as well as high-latitude regions of relatively high H I column density. After further excluding all cataloged external galaxies, we have isolated a sample with the highest probability of containing new classes of astronomical objects that could have been discovered only by *IRAS*.

## 2. *IRAS* OBSERVATIONS

### 2.1. *Sample Selection*

Our sources were extracted from the *IRAS Point Source Catalog* (see *IRAS Catalogs and Atlases* 1988, hereafter PSC), which lists sources positions and their flux densities in the 12, 25, 60, and 100 $\mu$m wavebands. Of the 245,000 sources in the PSC, 33,000 were detected only in the *IRAS* 100 $\mu$m band. Since upper limits were established in the other *IRAS* wavebands, sources detected only at 100 $\mu$m have spectra that rise steeply into the far-infrared. Such sources could not have been discovered before the *IRAS* survey, and thus they represented a new population of sources with unknown physical properties.

We developed a source list for further study using a two-stage selection process (Heiles et al. 1987). In the first stage, we included only those sources satisfying the following criteria: (1) high-quality (cf. *IRAS Explanatory Supplement* 1988) 100 $\mu$m flux densities brighter than 2 Jy, (2) ratio of flux density at

[1] University of California, Astronomy Department, Berkeley, CA 94720.
[2] NASA Goddard Space Flight Center, Code 685, Greenbelt, MD 20771.
[3] Seoul National University, Astronomy Department, Seoul 151-742, Korea.

100 $\mu$m to that at 60 $\mu$m greater than 5, and (3) absolute Galactic latitude greater than 10°. The total number of sources satisfying the first-stage criteria was about 20,000.

In the second stage of source selection, we included only those sources with *excess* 100 $\mu$m flux density, compared to the Galactic H I column density. The H I column densities were obtained from the Bell Labs survey (Stark et al. 1992) for Northern sources, or from the Parkes survey (Cleary, Heiles, & Haslam 1979) for Southern sources. From inspection of the 100 $\mu$m flux versus H I column density for the cirrus point sources, the criterion for infrared excess was determined:

$$F_{100} > N_{\rm HI}/8.66 \times 10^{20}\ {\rm cm}^{-2} - 0.625\ {\rm Jy}\ , \qquad (1)$$

where $F_{100}$ is the 100 $\mu$m flux density (Heiles et al. 1987). Note that the beam size of the H I surveys (120′ for Bell Labs, 48′ for Parkes) is much larger than the angular size of the *IRAS* sources (< 5′). Thus while sources satisfying equation (1) have a higher probability of not being associated with interstellar gas, those sources that fail to satisfy equation (1) are not necessarily clumps of interstellar gas. A total of 293 sources satisfied the first two stages of selection criteria. For the final selection criterion, we omitted all sources identified with known astronomical objects and clusters of sources in Orion, Ophiuchus, and Taurus. A total of 105 sources survived all selection criteria.

### 2.2. *Derivation of Infrared Properties*

We used several versions of the reduced *IRAS* data to determine the infrared properties of our sources. The *IRAS Point Source Catalog* (PSC) was produced by first median filtering the raw data stream (sky brightness as a function of time), then extracting sources that fit the point source template. The *IRAS Faint Source Survey* (Moshir et al. 1989, hereafter FSS) was produced by co-adding all *IRAS* observations *before* extracting sources, thus obtaining a sensitivity some 2.5 times bettter than the PSC. We extracted all sources in the FSS within 3′ of our PSC positions. The median ratio of FSS to PSC flux is 1.05 for sources with high-quality 100 $\mu$m fluxes.

Many of our sources are partially resolved, so the median filter used to detect sources in the PSC and FSS underestimates the total flux densities. The fact that our sources survived the stringent point source selection criteria demonstrates that they are smaller than the 100 $\mu$m cross-scan angular resolution (6′). However, the 60 $\mu$m and shorter wavelength emission can be resolved because of the smaller beam size at shorter wavelengths. Also, some sources are peaks of structures larger than the 100 $\mu$m in-scan angular resolution (3′), so the 100 $\mu$m flux is often underestimated. In order to determine accurate flux densities and spectra of the sources, it is necessary to determine (or limit) their angular sizes.

For intermediate-sized sources (2′–8′), the *IRAS Small Scale Structure Catalog* (1988, hereafter SSS) contains the best flux determination. We extracted all SSS sources within 6′ (or the estimated source size in the SSS, whichever was larger) of our sample positions. Corresponding entries were found for 61 sources, but only 43 of these had 100 $\mu$m fluxes. (The 18 SSS sources without 100 $\mu$m fluxes were accepted into the SSS based on partially resolved 60 $\mu$m flux; the 100 $\mu$m flux was unresolved and thus failed SSS criteria.) The median ratio of SSS to PSC 100 $\mu$m flux was 3.0. The ratio of SSS to PSC flux can be used to estimate the source size (cf. § V.B of the SSS), with the median ratio corresponding to a size of 5′. We conclude that a large fraction of our sources are extended to about 5′, and the PSC fluxes are underestimated even at 100 $\mu$m.

To determine the source sizes and infrared fluxes, we used the ADDSCAN and SCANPI programs to process the raw *IRAS* data (see IPAC User's Guide 1989). First, all survey scans passing within 2′ of the specified source position were retrieved and co-added to form a one-dimensional profile of the source. Then a parabolic baseline was subtracted from the profile. Finally, the baseline-subtracted profile was integrated to obtain the total flux, and the point source template was fitted to the data. We examined each profile and compared the point source template fits to the data for the four *IRAS* wavebands. If the point source template was a good fit at the shortest wavelength at which the source was detected, the source was deemed a "true" point source. For "true" point sources, the upper limit to the angular size was set to the approximate in-scan angular resolution for the shortest wavelength at which the source was detected (1′, 1′, 1.′5, and 3′ at 12, 25, 60, and 100 $\mu$m, respectively [FSS]). If a source appeared extended, relative to the point source template, then the angular size was estimated (to the nearest arcmin) from the profile at the shortest wavelength at which the source was detected.

The total infrared fluxes for our sources were calculated from the ADDSCAN profiles by integrating the surface brightness between the two zero-crossings nearest the specified position. As expected, the total fluxes are larger than the point source fluxes, with a median ratio of 100 $\mu$m ADDSCAN to PSC fluxes of 1.5. Comparison of ADDSCAN and SSS fluxes reveals good agreement for most sources: the mode of the flux ratio is $1.0 \pm 0.1$. There is an excess of sources with large SSS flux relative to the ADDSCAN flux; those sources flagged by the SSS as potential double point sources are the worst offenders. For those seven of our sources associated with large optical galaxies, we may compare our fluxes to those obtained by Rice et al. (1988), who integrated the flux over the entire extent of the galaxies using two-dimensional co-added maps. It is evident that the ADDSCAN fluxes are good estimates of the total flux for the three galaxies with optical diameters smaller than 10′, while the ADDSCAN fluxes are considerable underestimates (mean flux ratio of 1.9) for the four larger galaxies. The ADDSCAN procedure was also used by Helou et al. (1988) to determine the flux of a sample of Virgo cluster galaxies with optical isophotal diameters less than 2.′4; their results are in good agreement with those of Rice et al. (1988) for those galaxies in common. We conclude that the fluxes obtained by the ADDSCAN procedure are a good measure of the total flux of sources with angular size smaller than 10′.

The positions and infrared properties of our sources are listed in Table 1. Listed for each source are the following: column (1): sequential source number from our first-stage sample, preceded by "C" for cirrus; columns (2) and (3): right ascension and declination (1950.0) from the PSC, or from the FSS if available; columns (4) and (5): 100 and 60 $\mu$m flux from the PSC, or from the FSS if available; columns (6)–(9): 100–12 $\mu$m ADDSCAN fluxes; column (10): angular size, or the upper limit to the angular size, determined by examination of the source profile.

## 3. GROUND-BASED OBSERVATIONS

We have used a wide range of ground-based observational experiments in order to determine the nature of the unidentified far-infrared sources. The results of some optical imagery

TABLE 1

INFRARED PROPERTIES OF CIRRUS POINT SOURCES

| | | | *IRAS* FLUXES (Jy) | | | | | | |
|---|---|---|---|---|---|---|---|---|---|
| | | | PSC[a] | | ADDSCAN[b] | | | | |
| NAME (1) | R.A. (1950) (2) | DECL. (1950) (3) | $F_{100}$ (4) | $F_{60}$ (5) | $F_{100}$ (6) | $F_{60}$ (7) | $F_{25}$ (8) | $F_{12}$ (9) | SIZE $\theta$ (10) |
| 77..... | 00$^h$12$^m$39$^s$.4 | −00°38′57″ | 2.8 | 0.4 | 10.5 | 0.5 | ... | ... | 5′ |
| 80..... | 00 13 07.5 | −39 31 45 | 11.5 | 2.3 | 30.6 | 10.8 | ... | ... | 6 |
| 300..... | 00 44 40.9 | −25 38 33 | 29.1 | 3.3 | 90.7 | 17.3 | 1.5 | 1.8 | 3 |
| 309..... | 00 45 34.1 | −25 28 13 | 40.3 | 7.4 | 101.6 | 12.6 | 2.4 | 1.9 | 3 |
| 1065..... | 02 24 04.0 | +33 21 19 | 7.5 | 1.4 | 16.4 | 5.3 | 0.5 | 0.3 | 2 |
| 1220..... | 02 35 37.9 | −29 59 56 | 2.4 | 0.4 | 7.7 | 0.8 | ... | ... | 4 |
| 1236..... | 02 36 32.9 | −29 50 44 | 2.0 | 0.4 | 7.3 | 0.6 | ... | ... | 4 |
| 1248..... | 02 37 17.1 | −31 22 53 | 2.2 | 0.4 | 4.3 | 0.5 | 0.3 | 0.2 | 3 |
| 1321..... | 02 42 47.7 | −69 26 44 | 4.4 | 0.5 | 7.3 | 1.1 | ... | ... | 3 |
| 2671..... | 03 43 43.3 | +23 29 01 | 15.5 | 2.1 | ... | ... | 1.7 | 1.5 | 3 |
| 2716..... | 03 45 14.7 | +23 20 37 | 10.8 | 1.1 | 28.0 | 4.3 | 0.4 | 0.3 | 2 |
| 2983..... | 03 54 20.6 | +36 52 31 | 47.4 | 7.8 | 92.5 | 18.5 | 5.6 | 4.4 | 2 |
| 3486..... | 04 11 06.3 | +10 05 02 | 25.7 | 2.4 | 53.9 | 16.3 | 3.6 | 1.1 | 3 |
| 4055..... | 04 35 44.5 | −01 54 27 | 5.4 | 0.4 | 13.1 | 1.3 | 0.2 | ... | 3 |
| 4528..... | 04 58 41.9 | −09 01 27 | 7.3 | 1.0 | 4.6 | 1.3 | 0.2 | 0.2 | 3> |
| 4536..... | 04 59 06.6 | −08 56 32 | 17.3 | 2.5 | 43.4 | 7.0 | 1.1 | 0.3 | 1> |
| 4573..... | 05 00 24.0 | −08 22 52 | 6.1 | 0.9 | 8.3 | 2.2 | 0.7 | 0.5 | 2 |
| 4642..... | 05 03 16.3 | −06 57 06 | 11.7 | 1.6 | 33.3 | 11.0 | 1.3 | 1.1 | 4 |
| 4655..... | 05 03 50.7 | −04 00 31 | 15.9 | 0.8 | 43.5 | 8.5 | 0.5 | 0.2 | 4 |
| 4657..... | 05 03 54.1 | −06 26 05 | 10.0 | 1.2 | ... | 3.3 | 0.5 | 0.4 | 3 |
| 4665..... | 05 04 20.7 | −06 28 19 | 14.8 | 2.0 | ... | ... | ... | ... | 3> |
| 4880..... | 05 14 36.0 | −07 47 55 | 15.1 | 2.0 | 24.6 | 6.8 | 0.5 | ... | 2 |
| 4959..... | 05 17 46.0 | −05 44 39 | 21.3 | 3.3 | 38.3 | 7.0 | 1.2 | 0.5 | 2 |
| 4979..... | 05 18 31.9 | −05 52 37 | 26.0 | 1.6 | 48.6 | 13.5 | 1.1 | 1.0 | 3 |
| 4991..... | 05 18 59.3 | +07 28 47 | 24.2 | 0.9 | 24.3 | 8.2 | 1.3 | 0.8 | 2 |
| 5204..... | 05 26 44.8 | +12 25 05 | 28.3 | 2.1 | ... | ... | 3.0 | 2.4 | 2 |
| 5270..... | 05 28 40.2 | +12 03 13 | 69.2 | 9.2 | 137.1 | 20.8 | 4.8 | 9.2 | 1> |
| 5299..... | 05 29 32.7 | +12 47 33 | 47.6 | 9.1 | ... | ... | ... | ... | 0 |
| 5308..... | 05 29 51.6 | −26 31 34 | 2.0 | 0.4 | 4.3 | 1.0 | ... | 0.1 | 1> |
| 5431..... | 05 35 01.0 | −09 56 37 | 20.3 | 3.4 | ... | 7.5 | 0.8 | 0.8 | 1> |
| 5812..... | 05 49 30.0 | +00 46 28 | 28.7 | 3.9 | 60.7 | 11.8 | 2.1 | 1.7 | 2 |
| 5854..... | 05 51 30.2 | +01 50 08 | 27.3 | 3.8 | ... | 10.4 | 0.5 | 0.4 | 1> |
| 5937..... | 05 55 32.6 | −14 05 57 | 18.2 | 3.5 | 49.8 | 8.5 | 1.7 | 1.0 | 1> |
| 6897..... | 07 14 28.3 | −43 52 41 | 8.6 | 0.5 | 12.5 | 2.1 | 0.3 | 0.2 | 3 |
| 7117..... | 07 31 57.0 | −46 50 33 | 13.3 | 1.1 | 42.5 | ... | ... | ... | 4 |
| 7193..... | 07 37 50.5 | −47 45 17 | 12.8 | 1.8 | 29.9 | 4.7 | ... | ... | 3> |
| 7295..... | 07 46 18.7 | −49 40 37 | 11.3 | 1.1 | 32.0 | 4.0 | 0.3 | 0.4 | 2 |
| 7364..... | 07 53 31.0 | −50 29 29 | 14.2 | 1.1 | 25.2 | 6.7 | 1.4 | 0.5 | 3 |
| 7373..... | 07 54 19.6 | −50 29 03 | 18.3 | 2.4 | 32.1 | 5.3 | 0.7 | 0.4 | 2 |
| 8037..... | 09 17 05.4 | +69 32 16 | 3.5 | 0.4 | 6.0 | 0.7 | ... | ... | 3> |
| 8116..... | 09 30 13.7 | +66 24 01 | 3.7 | 0.4 | 8.7 | 0.5 | ... | ... | 3> |
| 8249..... | 09 47 26.7 | +71 09 15 | 3.1 | 0.4 | 8.1 | 0.8 | 0.1 | 0.1 | 2 |
| 8515..... | 10 37 18.7 | +73 36 53 | 5.0 | 0.4 | 7.6 | 1.6 | ... | ... | 3 |
| 8526..... | 10 40 29.4 | −36 04 44 | 5.3 | 1.0 | 7.2 | 2.1 | 0.4 | 0.5 | 2 |
| 8605..... | 10 49 44.1 | +25 14 23 | 2.0 | 0.4 | 4.2 | 0.7 | ... | ... | 4> |
| 8607..... | 10 50 10.1 | +25 12 51 | 5.1 | 0.5 | 12.7 | 0.9 | ... | ... | 4 |
| 8832..... | 11 26 46.5 | +63 52 49 | 2.2 | 0.4 | 2.1 | 0.5 | ... | ... | 3> |
| 8846..... | 11 29 37.8 | +64 16 52 | 2.3 | 0.4 | 5.1 | 1.0 | ... | ... | 3 |
| 8954..... | 11 48 32.9 | +58 56 01 | 2.4 | 0.4 | 4.7 | 0.7 | ... | ... | 3 |
| 8968..... | 11 49 24.0 | +61 45 06 | 3.0 | 0.6 | 6.8 | 1.0 | ... | ... | 3> |
| 8971..... | 11 49 43.3 | +61 39 52 | 2.0 | 0.4 | 2.9 | 0.8 | ... | ... | 3 |
| 8978..... | 11 50 41.9 | −09 46 22 | 2.9 | 0.4 | 8.3 | 0.7 | ... | ... | 3 |
| 9095..... | 12 07 41.6 | −51 57 40 | 9.0 | 1.0 | 12.8 | 3.0 | 1.0 | 1.3 | 3 |
| 9247..... | 12 31 56.9 | −05 15 19 | 2.2 | 0.4 | 5.2 | 0.3 | ... | ... | 3> |
| 9357..... | 12 54 44.5 | +09 05 13 | 2.0 | 0.4 | 2.6 | 1.2 | ... | ... | 3> |
| 9364..... | 12 55 31.9 | −21 24 32 | 2.2 | 0.4 | 8.1 | 1.0 | 0.3 | 0.2 | 2 |
| 9383..... | 12 58 39.6 | +21 20 56 | 2.2 | 0.4 | 5.9 | 0.7 | ... | ... | 3> |
| 9530..... | 13 24 49.8 | +16 24 18 | 2.1 | 0.4 | 5.9 | 1.0 | ... | ... | 3 |
| 9532..... | 13 25 07.2 | +16 23 23 | 2.8 | 0.4 | 6.1 | 1.2 | ... | 0.2 | 3> |
| 9605..... | 13 36 43.5 | +67 03 46 | 2.2 | 0.4 | 5.0 | 0.9 | 0.1 | ... | 3> |
| 9629..... | 13 40 59.9 | −07 57 09 | 2.5 | 0.4 | 6.7 | 0.7 | ... | ... | 3> |
| 9818..... | 14 07 19.0 | +20 52 02 | 2.7 | 0.5 | 6.6 | 1.2 | ... | ... | 3> |
| 9869..... | 14 15 07.5 | −43 01 27 | 6.1 | 0.9 | 8.0 | 2.7 | ... | ... | 3> |
| 10513..... | 15 21 45.8 | −32 39 50 | 17.1 | 0.9 | 31.2 | 3.2 | ... | ... | 3> |
| 10718..... | 15 31 45.6 | −26 45 43 | 17.3 | 1.4 | 35.7 | 4.9 | 1.3 | 0.3 | 3> |
| 10797..... | 15 35 02.1 | −24 45 12 | 11.1 | 0.9 | 21.6 | 3.8 | 1.1 | 0.5 | 4> |
| 10828..... | 15 35 59.9 | −33 15 37 | 13.7 | 1.0 | 31.0 | 3.8 | ... | ... | 3> |

TABLE 1—*Continued*

| Name (1) | R.A. (1950) (2) | Decl. (1950) (3) | *IRAS* Fluxes (Jy) PSC[a] $F_{100}$ (4) | PSC[a] $F_{60}$ (5) | ADDSCAN[b] $F_{100}$ (6) | ADDSCAN[b] $F_{60}$ (7) | ADDSCAN[b] $F_{25}$ (8) | ADDSCAN[b] $F_{12}$ (9) | Size $\theta$ (10) |
|---|---|---|---|---|---|---|---|---|---|
| 10859..... | 15 37 23.3 | −33 31 30 | 10.9 | 0.5 | 39.6 | ... | ... | ... | 4> |
| 10882..... | 15 38 03.6 | −27 29 21 | 15.1 | 2.0 | 19.2 | 6.2 | 1.1 | 0.7 | 3 |
| 10909..... | 15 39 12.4 | −25 21 29 | 19.8 | 2.1 | 40.4 | 10.0 | 0.8 | 0.4 | 3 |
| 10914..... | 15 39 19.3 | −26 10 12 | 17.0 | 1.9 | 35.3 | 7.4 | 0.3 | 0.4 | 3> |
| 10952..... | 15 40 58.0 | −33 12 08 | 14.4 | 1.3 | 40.0 | 4.2 | ... | 0.1 | 3> |
| 11119..... | 15 48 32.2 | −25 45 36 | 15.2 | 2.8 | 41.1 | 4.2 | 0.7 | 0.9 | 3> |
| 11610..... | 16 07 47.1 | −18 52 25 | 13.6 | 1.5 | 7.2 | 4.7 | 1.3 | 1.1 | 2 |
| 11617..... | 16 08 19.7 | −06 53 52 | 12.5 | 0.7 | ... | ... | ... | ... | 0 |
| 11846..... | 16 18 11.3 | −20 10 46 | 16.0 | 1.3 | ... | 7.9 | 1.3 | 0.5 | 3> |
| 11960..... | 16 23 01.8 | −15 53 60 | 19.3 | 2.0 | 44.2 | 8.3 | ... | ... | 3> |
| 12065..... | 16 27 06.7 | −19 37 29 | 15.5 | 2.4 | 26.9 | 9.4 | 1.6 | 0.7 | 2 |
| 12069..... | 16 27 14.0 | −19 53 53 | 16.1 | 3.0 | 32.2 | 7.8 | 1.0 | 0.9 | 1> |
| 12187..... | 16 31 32.1 | +61 22 02 | 2.3 | 0.4 | 4.9 | 0.4 | ... | ... | 3> |
| 12254..... | 16 33 56.3 | +61 35 34 | 2.6 | 0.4 | 3.2 | 0.3 | 0.1 | 0.1 | 3> |
| 12338..... | 16 37 13.6 | +64 45 37 | 2.1 | 0.4 | 6.4 | 0.6 | 0.1 | 0.1 | 3 |
| 12450..... | 16 40 44.0 | +51 30 35 | 2.1 | 0.4 | 4.1 | 0.3 | ... | ... | 3> |
| 12453..... | 16 40 57.9 | +60 30 44 | 2.1 | 0.4 | 4.8 | 0.4 | ... | 0.1 | 3> |
| 12457..... | 16 41 08.1 | +60 17 49 | 2.2 | 0.4 | 4.7 | 0.3 | 0.1 | 0.3 | 3> |
| 12547..... | 16 43 58.8 | −19 20 20 | 14.8 | 1.8 | 3.1 | 6.1 | 0.7 | ... | 3> |
| 12558..... | 16 44 16.7 | +60 09 30 | 2.5 | 0.4 | 2.1 | 0.2 | ... | ... | 3> |
| 12599..... | 16 45 27.6 | +37 34 59 | 2.4 | 0.5 | 8.9 | 0.9 | ... | ... | 3> |
| 12639..... | 16 46 57.7 | +61 25 11 | 2.1 | 0.4 | 3.4 | 0.4 | ... | ... | 3> |
| 12751..... | 16 51 42.4 | +61 15 19 | 2.5 | 0.4 | 5.4 | 0.6 | 0.1 | ... | 3> |
| 12811..... | 16 54 12.8 | +61 26 01 | 2.9 | 0.4 | 5.7 | 0.4 | ... | ... | 3> |
| 12899..... | 16 58 00.0 | +61 32 57 | 2.6 | 0.4 | 11.5 | 0.5 | ... | ... | 3 |
| 12902..... | 16 58 03.0 | +61 35 08 | 2.3 | 0.4 | 8.5 | 0.8 | ... | ... | 4 |
| 12920..... | 16 58 40.7 | +62 47 14 | 2.4 | 0.4 | 4.0 | 0.8 | ... | ... | 3 |
| 13101..... | 17 05 13.4 | +62 15 34 | 2.0 | 0.4 | 4.9 | 0.5 | ... | ... | 3 |
| 13135..... | 17 06 23.4 | +53 19 59 | 2.2 | 0.4 | 5.5 | 0.4 | ... | ... | 3> |
| 15331..... | 18 48 56.1 | −31 22 08 | 12.4 | 1.9 | 26.7 | 4.3 | 0.6 | 0.6 | 2> |
| 15615..... | 19 03 27.9 | −37 02 12 | 7.7 | 0.8 | 17.9 | 1.5 | ... | ... | 3> |
| 18768..... | 22 17 55.6 | −46 17 29 | 3.1 | 0.4 | 4.5 | 1.9 | ... | ... | 3> |
| 18755..... | 22 26 46.5 | −21 02 14 | 12.0 | 1.6 | ... | ... | ... | 0.5 | 2 |
| 18757..... | 22 26 59.4 | −21 09 38 | 13.3 | 2.3 | ... | 8.7 | ... | ... | 3> |
| 18759..... | 22 27 07.7 | −21 01 39 | 11.6 | 1.1 | 33.5 | 8.3 | ... | ... | 3> |
| 18760..... | 22 27 27.8 | +40 05 58 | 14.1 | 1.8 | 25.5 | 3.9 | 0.9 | 0.5 | 2 |
| 18963..... | 22 50 19.2 | +24 29 11 | 5.6 | 0.4 | 11.0 | 2.0 | 0.4 | ... | 1> |
| 19228..... | 23 07 57.7 | −27 10 29 | 2.2 | 0.4 | 4.7 | 0.5 | ... | ... | 3> |

[a] Fluxes from the *Point Source Catalog* (1988).
[b] Integrated fluxes from the ADDSCAN program (see text).

using the 120″ telescope at Lick Observatory[4] have already been reported (Heiles et al. 1987); out of eight infrared sources observed, three were found to have likely extragalactic counterparts, two had indications of cirrus-like nebulosity, and three had blank optical fields. In the following sections, we describe the radio continuum, H I 21 cm, and millimeter-wave spectral-line observations that eventually allowed us to characterize the infrared sources.

### 3.1. *Radio Continuum Observations*

We surveyed nearly all of our unidentified sources for radio continuum emission. Images of the fields containing 54 cirrus point sources were obtained at the NRAO[5] Very Large Array (VLA) on 1987 April 18 and 21. The array was in the D (most compact) configuration, and the beam size and field of view were ∼40″ and 30′, respectively. The central frequency and bandwidth were 1464.90 and 50 MHz, respectively. Each source was observed for 5–10 minutes, yielding a "snapshot" image, with sparse but reasonably uniform coverage of the *u-v* plane. Primary calibration was tied to 3C 286, with an assumed flux density of 14.5 Jy. Phase drifts were removed by observing bright sources about every 20 minutes.

Data reduction was performed using the Astronomical Image Processing System (AIPS). First, maps of the central 20′ of each field were constructed with 10″ cell size. The synthesized beam was deconvolved from all sources in the field using the AIPS program MX. This program transforms the *u-v* data into the image, identifies the CLEAN components, and subtracts the FFT of the beam from the *u-v* data at each iteration. It was immediately evident that there were a large number of sources in the beam, and at least 100 iterations were needed to reduce the correlated pseudo-noise created by sidelobes of bright sources down to the 2 mJy level. Since the receiver noise was only ∼0.2 mJy, the main limitation to the sensitivity was confusion. For about half of our sources, the cleaned 20′ maps were contaminated by bright sources beyond the FWHM of the primary beam. These maps were reconstructed by cleaning a larger, 40′ field, requiring up to 500 iterations in some cases.

[4] Lick Observatory is operated by the University of California at Santa Cruz.
[5] The National Radio Astronomy Observatory is operated by Associated Universities, Inc., under Cooperative Agreement with the National Science Foundation.

TABLE 2

VLA 1400 MHz CONTINUUM FLUXES

| Source | $F_\nu(2' \times 2')$ (mJy) | $I_\nu$(peak) (mJy beam$^{-1}$) | $\theta$(VLA-*IRAS*) |
|---|---|---|---|
| 4642[a] | 2.1 | 2.9 | 0.8 |
| 4665[a] | 6.3 | 3.8 | 0.2 |
| 4991[a] | 6.4 | 5.4 | 0.6 |
| 8515 | 3.9 | 3.4 | 0.8 |
| 8954 | 1.9 | 0.9 | 0.8 |
| 9629 | 6.6 | 3.9 | 0.3 |
| 10797 | 4.7 | 1.2 | 0.4 |
| 10914[a] | 8.5 | 1.4 | 1.2 |
| 12599 | 3.6 | 3.2 | 0.6 |
| 15615 | 3.7 | 2.2 | 0.4 |
| 18755[a] | 40.6 | 8.0 | 0.9 |
| 18757[a] | 20.9 | 6.2 | 1.4 |
| 18963 | 2.9 | 2.5 | 0.8 |

[a] The aperture over which the flux was integrated for this source was increased to $4' \times 4'$ to include the entire synthesized beam, which was elongated to 2′ along its major axis.

Due to the large number of extragalactic radio sources at 1400 MHz, it is possible that the radio sources near the *IRAS* position are associated by chance. For the central 10′ of each map, we determined the peak surface brightness (mJy beam$^{-1}$) and the angular separation between the peak and the *IRAS* position. The peak brightnesses were typically 25 mJy beam$^{-1}$, and nine fields had sources brighter than 50 mJy in the central 10′. The distribution of the angular separations between the peaks and the *IRAS* positions is consistent with sources placed in the field randomly. Using the cumulative source counts of Oosterbahn (1978) and Condon (1984), the probability of finding a 25 mJy source in a $10' \times 10'$ area is about 50%.

Fortunately, the *IRAS* positions are accurate to about 1′, and the *IRAS* source sizes are less than 5′. In order to determine whether a radio continuum source is associated with an *IRAS* source, we calculated the total flux (mJy) and identified the cell with the highest brightness (mJy beam$^{-1}$) within the central 2′ of each VLA map. If the total flux within the 2′ aperture was greater than 80% of the peak flux/beam, then excess radio emission was detected at the *IRAS* position. Excess radio emission was detected for 13 *IRAS* sources. If the total flux was less than the peak flux, but greater than 1 mJy, then there may be emission from the *IRAS* position; the background surface brightness in the center of the map was negative due to sidelobes from nearby sources. Potential excess emission was detected from seven *IRAS* sources. Upper limits were established for 34 *IRAS* sources with total radio flux less than 1 mJy. The radio fluxes of potential detections are listed in Table 2.

### 3.2. *Radio Spectral-Line Observations*

Observations of the 1420.4058 MHz line of H I were performed at the NAIC[6] Arecibo 305 m telescope in 1985 December, 1987 October, and 1990 April. The "dual circular" feed, which illuminates the central 200 m of the dish, was used to obtain 3′ resolution and to detect both polarizations. For a backend, we used the 2048 channel autocorrelator with a bandwidth of 2.5 MHz per polarization, yielding a velocity coverage of 500 km s$^{-1}$ and a resolution of 0.5 km s$^{-1}$. Total power spectra were obtained at each position, and frequency-switched spectra were derived by observing the same position with a velocity offset of +600 km s$^{-1}$ (2.8 MHz). For mapping observations, the same off-frequency spectrum was used for each map position; the stability of the system and atmosphere were excellent over periods of several minutes. An integration time of 30 s was enough to obtain rms fluctuations of about 0.1 K in the spectra. A correction was applied to all spectra taken at zenith angles greater than 10°. For higher zenith angles, part of the 21 cm feed illumination pattern falls off the 305 m reflector, increasing the system temperature and beamwidth. The zenith-angle dependence was determined by observing the central position of scans and maps repeatedly; the functional form is reasonably approximated by $1 + (ZAC - 1)/2$, where $ZAC$ is the correction factor for point sources. The brightness temperatures and peak column densities reported below have been divided by a beam efficiency of 0.78, to correct for the substantial power contained in distant sidelobes of the 21 cm feed.

Results of the 1985 observing run have already been reported (Heiles et al. 1987). In summary, we observed 17 sources, including six unidentified sources from Table 1 (C8605, C9357, C9364, C9383, C9530, and C9532) as well as sources with catalog associations. The excess Galactic H I column density at the *IRAS* position was measured by observing a hexagonal pattern with 3′ offsets, and subtracting the average of the off-source spectra from the central, on-source spectrum. The excess column densities for all sources was smaller than $3 \times 10^{19}$ cm$^{-2}$. (For the 6 sources in Table 1 the excess column densities were 1.0, −0.3, 1.8, 2.4, −3.2, and $3.0 \times 10^{19}$ cm$^{-2}$, respectively.) In order to determine whether the sources were uncataloged external galaxies rich in interstellar material, we searched for redshifted H I lines out to 17,000 km s$^{-1}$ using the tuneable 22 cm feed. Extragalactic H I lines were detected for six sources, all of which were associated with known spiral galaxies (UGC 5864, 7074, 7284, 8041, 8421, and 8713). None of the unidentified *IRAS* source positions revealed extragalactic H I lines out to 17,000 km s$^{-1}$.

During the 1987 observing run, we observed 12 unidentified *IRAS* sources from Table 1 in the range of declinations accessible from Arecibo (and excluding the Orion-Taurus region). The sources can be broken up into three close pairs (separation less than 6′) and six isolated sources. For all sources, we observed a small map, consisting of a pattern of 12 points separated from the *IRAS* position by half the Arecibo beamwidth. From these small maps we measured the excess H I column density at the *IRAS* source position. The Arecibo and *IRAS* 100 $\mu$m resolutions are well matched for this experiment.

We also observed 1° long scans in right ascension and declination, with a spacing equal to the Arecibo beamwidth (3′), for each source, and we mapped the H I in the vicinity of the three pairs of sources. The central position was observed at the beginning and end of each scan and map, in order to check the dependence of the aperture efficiency on zenith angle. There was never a simple peak at the *IRAS* position. However, the H I column density as a function of offset from the *IRAS* position revealed the existence of substantial *gradients*, and there were small excess column densities at some positions. The excess column density was measured by subtracting the average of the small map OFF spectra from the central spectrum; the results are shown in Table 3. In the following subsections we describe the H I distribution in the vicinity of each source.

*C1065*—This source is actually the nucleus of the nearby,

[6] The National Astronomy and Ionosphere Center is operated by Cornell University under contract with the National Science Foundation.

TABLE 3

TOTAL AND EXCESS[a] H I COLUMN DENSITIES

| Source | Total $N$(H I) $10^{20}$ cm$^{-2}$ | Excess $N$(H I) $10^{20}$ cm$^{-2}$ |
|---|---|---|
| 1065[b] | 5.4 | 0.2> |
| 2716 | 10.9 | 0.2> |
| 8607[c] | 0.9 | 0.1> |
| 8607[c] | 3.6 | 0.3 |
| 9357[d] | 0.4 | 0.1> |
| 9357[d] | 0.4 | 0.3 |
| 9364 | 5.0 | 0.9 |
| 9383 | 4.7 | 0.5 |
| 9532 | 1.0 | 0.3 |
| 9818 | 3.7 | 0.2> |
| 12599 | 2.9 | 0.2> |
| 18963 | 5.1 | 0.2> |

[a] Excess column density is the column density observed at the *IRAS* position minus the average of the column density observed at positions separated 1 beam away (N, S, E, and W).

[b] The total and excess column densities listed here are for Galactic H I ($v_{LSR} < 150$ km s$^{-1}$). The external galaxy NGC 925, which is the likely counterpart of the *IRAS* source, is discussed in the text.

[c] The first line lists column densities in the low-velocity line, and the second line is for the intermediate-velocity line ($-45$ km s$^{-1}$).

[d] The first line lists column densities in the low-velocity line, and the second line is for high-velocity line ($+133$ km s$^{-1}$).

bright galaxy NGC 925, which escaped notice in the PSC and in our own preliminary inspection of the Palomar Observatory Sky Survey. The redshifted H I line, at 550 km s$^{-1}$, was detected as a negative line, nearly centered in the frequency-switched spectrum. We mapped the H I distribution of the galaxy and found that the *IRAS* source is coincident with the H I peak and the optical nucleus. The extent of the H I (full width at half the peak column density) is 12′ × 6′, which is also the extent of the visible disk of the galaxy, and the rotation velocity is about 180 km s$^{-1}$. The peak column density of NGC 925 is $8.3 \times 10^{20}$ cm$^{-2}$. The *IRAS* properties in Table 1 refer to the same region as the brightest spectrum in the galaxy, since the source size is the same as the Arecibo beam size. From the ratio of infrared flux to the H I flux, we find that the infrared emission per H atom in the central region of NGC 925 is about 1.5 times greater than in the solar neighborhood. This excess is probably due to either somewhat brighter interstellar radiation field in NGC 925, or to the fact that we have not included $H_2$ in the inventory of H nuclei, or both.

*C2716*—There is a sharp gradient in the H I column density as a function of declination across this source. The amplitude of the gradient is 27% (over 1°) of the column density at the *IRAS* position. The source is at the edge of the reflection nebula surrounding the Pleiades.

*C8605 and C8607*—These sources are associated with a bright intermediate-velocity cloud (IVC) at $-40$ km s$^{-1}$. We made a 30′ × 30′ map of the cloud at 3′ resolution. There is no structure in the low-velocity gas at the 10% level, and the column density of low-velocity gas is four less than the intermediate-velocity gas. The *IRAS* sources do not coincide with the peak H I column density of the IVC, but they are located only 15′ away and C8607 is associated with a secondary maximum in the H I.

*C9357*—A high-velocity cloud (HVC) at $v_{LSR} = +133$ km s$^{-1}$ was discovered in the Arecibo scans through this source. There is no structure in the low-velocity H I, and the total column density of low-velocity gas is among the lowest in the sky. The HVC peak is offset from the *IRAS* position by ~2 Arecibo beams, so the association is uncertain. If the *IRAS* source and HVC were associated, then this would be the first case that infrared emission was detected from a high-velocity gas, despite careful searches (Wakker & Boulanger 1986). During the 1990 observing run, we mapped the entire 1° × 1° field for high-velocity H I. For extra sensitivity and baseline stability (sacrificing only unneeded velocity resolution), we used a 5 MHz band width and switched frequencies by half the bandwidth, so that the spectral line was observed continuously. The results are shown in Figure 1. High-velocity gas was present in at least five clouds in the field. The brightest HVC was centered 5′ from the *IRAS* position, with a size of about 10′ × 10′. We performed deeper H I observations at the positions of minor peaks in the *IRAS* maps, and detected the high-velocity line at most positions. However, the H I column density was not correlated with the infrared surface brightness, and the peaks of the two maps do not coincide. We have therefore concluded that the *IRAS* emission is not associated with the HVC. Using star positions from the *Guide Star Catalog* (Jenker et al. 1989), a precise optical overlay was created and the position of a faint galaxy on the Palomar Observatory Sky Survey, near the *IRAS* position, was measured. An optical image of the field revealed a spiral galaxy near the *IRAS* position, and the optical spectrum contains [O I], Hα, [N II], and [S II] lines at a redshift of 0.057 (M. Dickinson 1991, personal communication). At that redshift, the *IRAS* flux corresponds to an infrared luminosity of $2.7 \times 10^{10}$ $h^{-2}$ $L_\odot$, compared to the estimated optical luminosity of $6 \times 10^9$ $h^{-2}$ $L_\odot$. The offset from the *IRAS* position is 39″ ± 16″. We conclude that this *IRAS* source is likely to be associated with the external galaxy. There is no infrared emis-

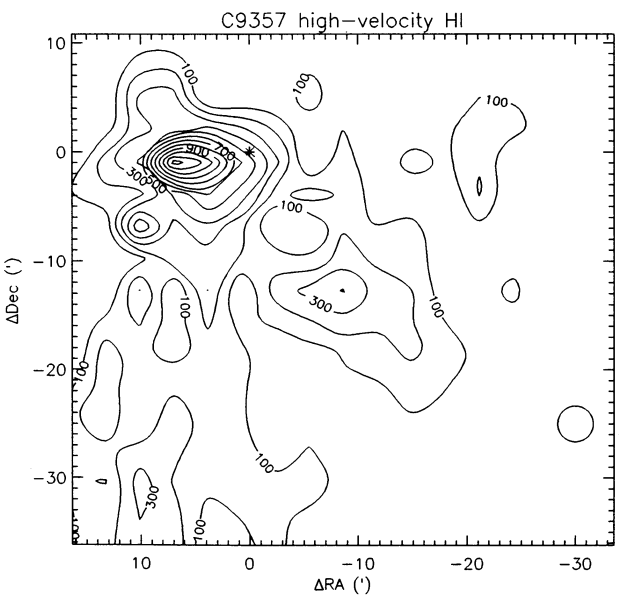


FIG. 1.—Map of the high-positive-velocity (115–150 km s$^{-1}$) H I column density observed at Arecibo in the vicinity of cirrus point source C9357. The *IRAS* position is indicated by an asterisk. The angular separation between the H I and *IRAS* peaks is 5′.5 ± 1′.5. A faint galaxy is visible on the Palomar Observatory Sky Survey prints, 0′.7 ± 0′.3 from the *IRAS* position.

sion correlated with the high-velocity clouds in our map, but our observations place only a weak limit on the gas-to-dust mass ratio (less than 25 times the value in the Galactic plane).

*C9364 and C9383*—The H I was mapped in a 60′ × 30′ field surrounding this pair of sources, revealing a very thin filament of H I. The H I and *IRAS* 100 μm maps are shown with identical pixel centers in Figure 2. The H I extends across the map in right ascension but is only about 12′ wide in declination. The contrast between the filament and the background is 40% of the peak column density. The *IRAS* sources correspond to two peaks along the filament. The *IRAS* scanning direction was perpendicular to the filament, so the point source detection algorithm was tricked into detecting a string of pseudo-point sources.

*C9530 and C9532*—We mapped the H I in a 30′ × 30′ field around this very close pair of sources. The two sources are associated with the peak of a thin H I filament. The column density contrast between the filament and the background is 30% of the peak column density. The spectral lines contain both a very narrow (3 km $s^{-1}$ FWHM) component and broader wings, with about 10 times as much column density in the narrow component.

*C9818*—Scans through the *IRAS* position revealed a mild (10%) gradient in the H I column density toward the NE. But the excess H I at the *IRAS* position relative to adjacent beams was less than 5% of the total.

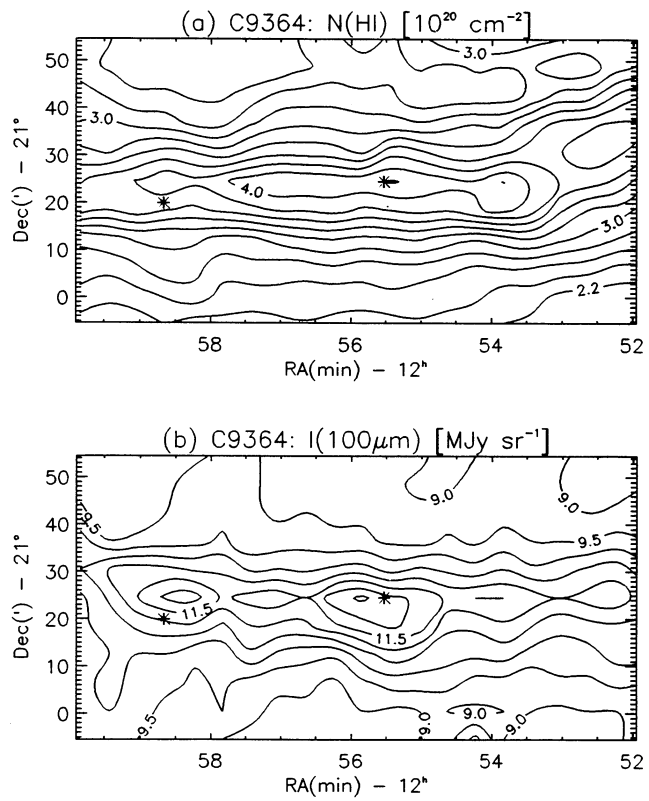


FIG. 2.—Maps of the H I column density observed at Arecibo (*a*) and 100 μm surface brightness observed by *IRAS* (*b*) in the vicinity of cirrus point sources C9364 and C9383, which are marked by asterisks. These sources are associated with a filamentary interstellar cloud. The cirrus point sources are located in the ridge of maximum H I column density. The cirrus point sources are produced by dust in two molecular clumps that have formed in the high column density ridge.

*C12599*—There is no small-scale structure (at the 8% level) in the H I near this *IRAS* source.

*C18963*—There is a sharp drop in the H I column density across this source; the amplitude of the gradient is 42% (over 1°) of the column density at the *IRAS* position. The gradient extends across the mapped region, and there is no evidence of a "hole" in the H I at the cirrus point source position. This ISM around this source is part of the large galactic shell GS 90-28-17 (Heiles 1984), and the *IRAS* source is located at the edge of a dense cloud just inside the inner edge of the H I shell. Thus there is strong evidence that a shock has passed through the region, and the higher density gas may still be experiencing a shock. In addition to the H I line observations, we used the 1665 MHz feed at Arecibo to search for OH lines at the *IRAS* position, and we detected both the 1665.402 and 1667.358 MHz lines at antenna temperatures of $0.06 \pm 0.012$ and $0.10 \pm 0.012$ K, respectively, with widths of $1.3 \pm 0.3$ km $s^{-1}$. The ratio of the brightnesses of the 1667 and 1665 MHz lines is $1.7 \pm 0.5$. The excitation temperature of the Λ-doublet levels of OH in interstellar clouds is difficult to determine from observations of the emission lines alone. But if our cloud is similar to those studied by Crutcher (1979), then the low brightness temperature of the lines is likely due to low optical depth, rather than being due to excitation at nearly the same temperature as the background. If the excitation temperature is comparable to the kinetic temperature implied by the CO lines (discussed below), then the OH column density may be derived: $N(\mathrm{OH}) \simeq 8 \times 10^{13}$ $\mathrm{cm}^{-2}$. Comparison to the CO column densities and $H_{tot}$ column densities inferred below indicate an abundance $N(\mathrm{OH})/N(H_2) \simeq 3 \times 10^{-8}$, similar to the OH abundances obtained for dark clouds by Crutcher (1979).

### 3.3. *Millimeter-Wave Spectral-Line Observations*

#### 3.3.1. *Kitt Peak*

We observed the 115.27120 GHz rotational transition of CO ($J = 1$–0), as well as the 110.20135 GHz rotational transition of $^{13}$CO ($J = 1$–0), during two observing runs at the NRAO 12 m telescope on Kitt Peak. The 3 mm SIS receivers were used in conjunction with a 512 channel filter bank spectrometer, with one receiver for each linear polarization. The observed spectra consist of four 128 channel sections: for each receiver, two filter banks with different resolutions were used in parallel. The observing strategy during the first observing run (1987 July 6–11) was to search a wide range of velocities for detection purposes. Thus we observed the CO (1–0) line, using the 250 kHz filters for reasonable resolution (0.65 km $s^{-1}$) and the 500 kHz for a broad velocity coverage (166 km $s^{-1}$ total). During the second observing run, we observed both the CO and $^{13}$CO lines, using the narrower 100 kHz filters (0.26 km $s^{-1}$ resolution) in order to fully resolve the lines. The beam size of the telescope at 115 GHz is 1′, and the aperture efficiency is 0.44. Absolute calibration was achieved by observing a moveable, room-temperature flap that was placed in the optical path between the secondary reflector and the receiver every 4 minutes. Typical system temperatures at 115 GHz were 400–600 K during the 1987 observing run and 700–1000 K during the 1988 observing run; typical system temperatures at 110 GHz were 500–600 K during the 1988 observing run.

Astronomical continuum sources (Jupiter, 3C 273, DR 21, and 3C 84) were observed to obtain pointing offsets and optimal focus. Also, several spectral line sources were observed using the same backend as used for our selected *IRAS* sources.

There was a calibration difference between the two observing runs, such that the $T_R^*$ obtained during the 1988 run was $1.39 \pm 0.04$ times brighter than during the 1987 run. An anomaly in the antenna temperature scale at the NRAO 12 m in the summer of 1988 was also noted by other observers and has since been corrected (P. Jewell 1990, private communication). Antenna temperatures from the 1988 observing run were divided by 1.39 to obtain $T_R^*$ in the tables and figures. We chose IRC +10216 as a secondary calibrator, for use in fixing the relative calibration between the two observing runs at the NRAO 12 m and the observations with the HCRO 6 m (discussed below). The coupling efficiency between the NRAO 12 m telescope and the brightness distribution of IRC +10216 was calculated using the measured properties of the telescope beam at 115 GHz ($\eta_M^* = 0.82$ with an error beam FWHM of 16′; Jewell 1988) and the observed brightness distribution of the source (2.′1 FWHM Gaussian [Ulich & Haas 1976, from the NRAO 11 m]; and 2.′6 FWHM [A. Stark 1990, private communication; from the Bell Labs 7 m]). We obtain a beam coupling efficiency of $\eta_f = 0.70$, where $\eta_f$ relates $T_R^*$, the antenna temperature corrected for ohmic losses and aperture efficiency, to $T_b$, the brightness temperature of the source, through $T_R^* = \eta_f T_b$. Dividing our observed IRC +10216 antenna temperatures, from the 1987 observing run, by the beam coupling efficiency yields a brightness temperature of 10.5 K.

Observations of our sources were performed by alternately observing the source position and a reference position. The reference positions were 60′ away during the 1987 observing run; about half of the reference positions were shifted in declination, and half in azimuth. The source and reference positions were observed for 1 minute each, two on-off pairs were accumulated, and the two receivers were averaged, resulting in fluctuations in the spectra of typically 0.15 K (rms). During the 1988 observing run, reference positions were chosen based on the location of interstellar clouds on the *IRAS* sky maps; the reference offset was typically 30′. Sources with strong spectral lines were only observed for 2 minutes, while fainter sources were observed longer. Some bright sources were mapped and found to be extended.

Additional observations of the CO emission of 10 sources were made in 1990 May in order to test for the presence of low-level wings in the spectral line profiles. These observations were performed in the beam-switching mode, with the secondary reflector switching between the source position and a position 6′ away (in azimuth). Every minute, the telescope was pointed 1° north of the source, and a beam-switched observation of the presumed-blank reference position field was performed. The final spectrum is the difference between the beam-switched spectra of the source and reference. It was not necessary to subtract a baseline from the spectra, because the rapid, small-offset beam switching eliminated time-variable receiver response and time- and spatial-variable atmospheric brightness. Some of the sources show evidence of extended emission. The intensity drops to negative values where the 6′ away reference position has more emission than the central position. Thus these spectra are not useful for absolute brightness temperatures; they are, however, extremely sensitive to emission outside the line core, as long as such emission is not uniformly bright over a larger than 6′ region. Spectra were obtained at 0.26 and 1.30 km $s^{-1}$ resolution, the latter being highly sensitive to extended wings. Results for some of the sources are shown in Figure 3; they are clearly negative—no extended wings are present. Note most of the observed sources are part of the Draco nebula, and lack of wings suggests these sources are not protostars in the outflow stage of evolution.

#### 3.3.2. *Hat Creek*

Both the CO (1–0) and $^{13}$CO (1–0) lines were observed for 25 of our sources using antenna 1 of the Hat Creek Radio Observatory millimeter-wave interferometer. This observing project, which occurred during 1990 May 12–17, occurred while one of the other elements of the interferometer was under repair. The antenna has a diameter of 6 m, and a beam width of 2′ at 115 GHz. The backend is a 512 channel correlator, which we set up with 256 channels each at bandwidths of 40 and 10 MHz in parallel. The total velocity range covered was 100 km $s^{-1}$ (with the 40 MHz bandwidth), and the velocity resolution in the central 26 km $s^{-1}$ of the spectrum was 0.10 km $s^{-1}$ (with the 10 MHz bandwidth). Observations were performed by alternately observing the source and a reference position for 1 minute each. The reference positions were chosen to be 60′ north of source. Three of the spectra revealed contamination in the reference position; these sources were reobserved with a reference position 60′ to the south.

Absolute calibration was achieved by observing Jupiter; we obtained an aperture efficiency of $\eta_A = 0.45 \pm 0.1$. The aperture efficiency was the same at 110 and 115 GHz to within the measurement uncertainties. As a secondary calibration, we observed the CO line of IRC +10216 and found an antenna temperature of $T_A = 1.9 \pm 0.1$ K. In order to compare the antenna temperature scale with that of our Kitt Peak observations, we must correct for the beam coupling efficiency of the Hat Creek telescope. The error beam amplitude was determined by observing several positions offset from the center of the Sun by 0′, 10′, 14′, 20′, and 28′. Each measurement was an on-off pair, with the reference position 60′ away in azimuth. If the error beam FWHM is 20′ we derive a corrected main beam efficiency of $\eta_M^* = 0.66 \pm 0.1$. Using the observed brightness distribution of IRC +10216, the beam coupling efficiency is $\eta_f = 0.40$. Dividing our observed $T_A$ by $\eta_A \eta_f$, we obtain a brightness temperature for IRC +10216 of $11 \pm 2$, in good agreement with the brightness temperature derived from our Kitt Peak measurements. Once the aperture and beam coupling efficiencies are properly accounted for, the brightness temperatures obtained with the NRAO 12 m telescope can be compared to those obtained with the HCRO 6 m antennas.

One source, C4655, was mapped in $^{13}$CO using the HCRO 6 m; we observed a $5 \times 5$ beam grid with 2′ (full-beam) spacing. The peak line temperature at HCRO was $T_R \simeq 11 \pm 2$ K, comparable to the $13 \pm 1$ K obtained at NRAO. The line temperature diminishes rapidly, to less than 2 K, to the S and E of the *IRAS* position, but the emission extends about one beam to the N and at least two beams to the W. The extended emission is about half as bright as the peak centered on the *IRAS* source. This source is embedded in a bright globule (LBN 923), and the *IRAS* source we selected is near the E edge, in agreement with the CO map. The nebulosity extends to the W and includes another *IRAS* source that has detectable 12 μm *IRAS* flux of 2.4 Jy (derived from survey COADDs). The globule was selected optically by Clemens & Barvainis (1988), who have observed the CO line with the MWO 6 m ($T_R = 14$ K); subsequent observations revealed no evidence for an active outflow (Yun & Clemens 1992). It seems that C4655 is embedded in a globule with another protostar at a somewhat later stage of development.

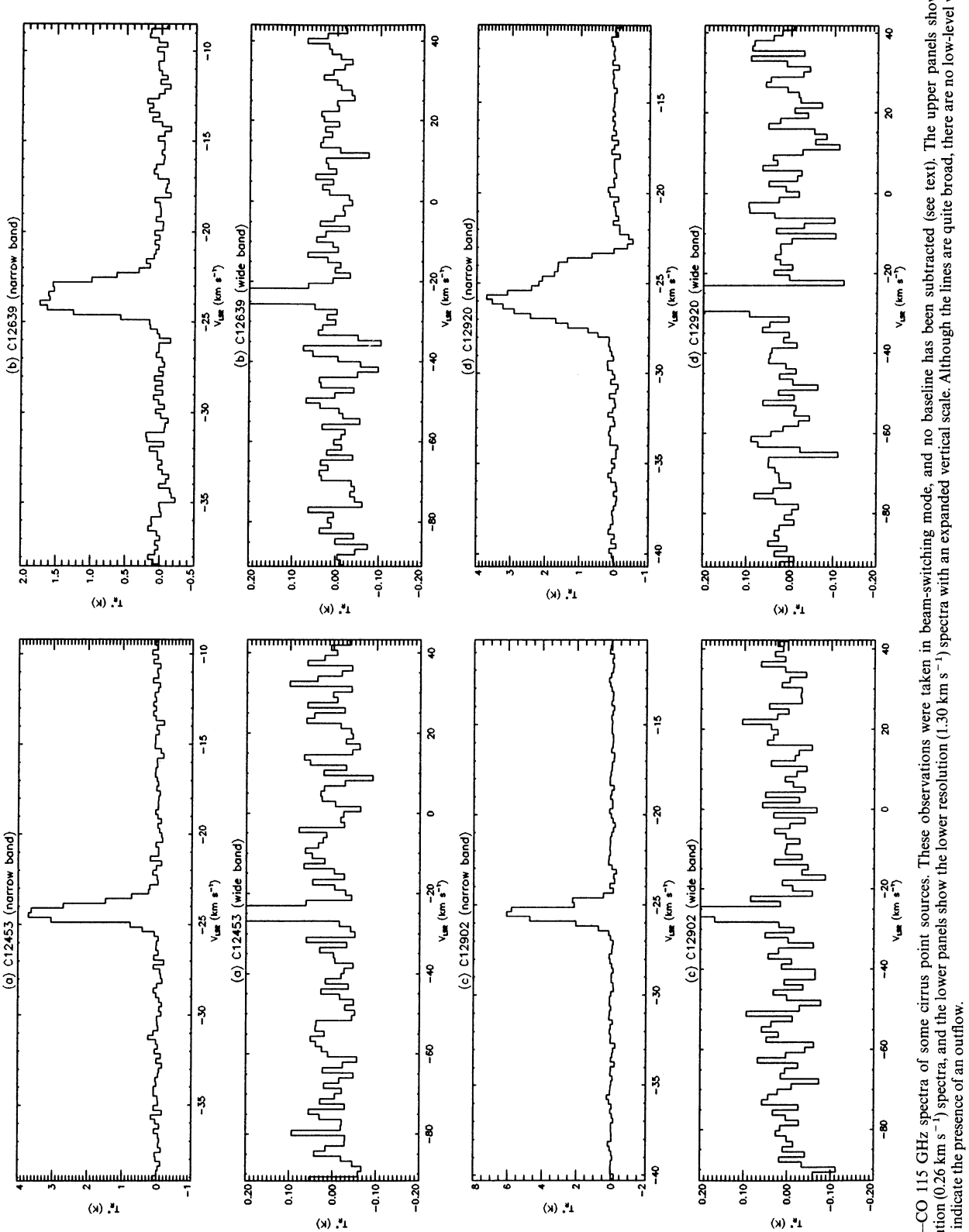


FIG. 3.—CO 115 GHz spectra of some cirrus point sources. These observations were taken in beam-switching mode, and no baseline has been subtracted (see text). The upper panels show the high-resolution (0.26 km $s^{-1}$) spectra, and the lower panels show the lower resolution (1.30 km $s^{-1}$) spectra with an expanded vertical scale. Although the lines are quite broad, there are no low-level wings that would indicate the presence of an outflow.

### 3.3.3. *Five Colleges*

Six sources with bright CO lines were observed in 1991 December with the 14 m telescope of the Five Colleges Astronomy Observatory (FCRAO). The 15 beam QUARRY backend was used, so that 15 spectra of 32 channels each were obtained simultaneously. The width of each channel was 250 kHz (0.7 km $s^{-1}$)—insufficient to fully resolve the lines. Further, the observations were performed while snow covered part of the radome that encloses the telescope, so the absolute intensity scale is calibrated to only ~30% accuracy. However the maps of the integrated line intensity are a reliable indicator of source morphology, and the absolute intensities were already measured with other telescopes. Two pointings of the QUARRY system allow one footprint, a region 4.′17 × 5′, to be mapped with 50″ (full beam) spacing. A single reference observation was performed for each footprint. Two sources were observed in single-footprint (30 spectra) maps (C4055 in $^{13}$CO, and C13135 in CO), and four sources were mapped using multiple footprints (C5270, 360 $^{13}$CO spectra; C8116, 360 $^{13}$CO spectra; C11617, 150 $^{13}$CO spectra; C12547, 150 CO and 60 $^{13}$CO spectra). The maps are shown in Figure 4. In all cases there is either a clear molecular-line peak, or, in the case of C5270, a very strong ridge. The molecular clumps are typi-

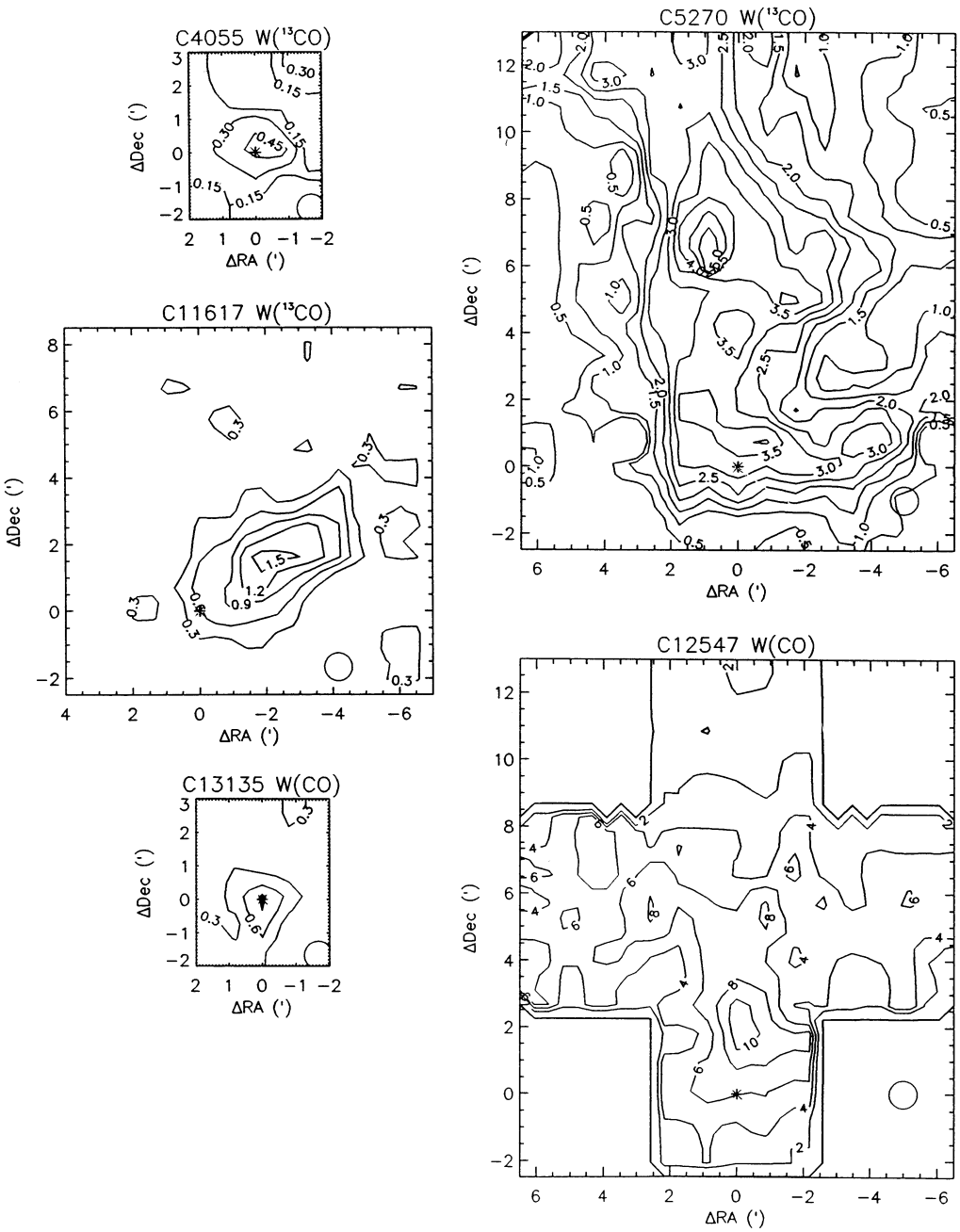


FIG. 4.—Maps of the integrated CO line intensity observed at FCRAO using the 15 beam system, for (*a*) C4055, (*b*) C5270, (*c*) C11617, (*d*) C13135, and (*e*) C12547. The isotope is indicated at the top of each map, and the contours are labeled in units of K km $s^{-1}$, where the temperature scale is antenna temperature ($T_A^*$). The *IRAS* positions are indicated by the asterisks, and the beam is indicated as a circle in the corner.

cally ~3′–8′ in size, and the peaks are offset from the *IRAS* positions by typically ~3′. The offsets are comparable to the *IRAS* 100 μm beam but sometimes larger than the *IRAS* positional uncertainty; these offsets are most likely due to the inability to disentangle high-spatial-frequency structures in a complicated cloud.

#### 3.3.4. *Summary of CO Data*

Each well-detected spectral line was fit by one or more Gaussians. The results of the millimeter-wave spectral line observations are presented in Table 4, where the temperature, LSR velocity, and FWHM line width are listed for 36 sources for which both the CO and $^{13}$CO lines were observed. (An additional 41 sources were observed for $^{12}$CO only.) Uncertain CO line profile fits are indicated by colons, and upper limits (equal to twice the rms) are indicated by "<." The temperatures listed in the table are $T_R^*$, that is, corrected for aperture efficiency but not corrected for beam coupling efficiency. The beam coupling efficiency can be estimated only for mapped sources. For all sources with estimable angular size (from the *IRAS* observations), the beam coupling efficiencies calculated using the main diffraction and error beams of the appropriate telescope are very near unity, since the millimeter-wave observations have higher resolution than *IRAS*. For sources unresolved in infrared, the beam coupling efficiency for the upper limit to the source size is nearly unity, but in principle the millimeter-wave observations yield only a lower limit to the brightness temperature.

The non-Gaussian character of many of the line profiles is indicated in Table 4 by a symbol appended to the line width. Lines with complicated profiles that cannot be decomposed into three or fewer Gaussians are indicated by a "C"; lines that are closely blended double-peaks are indicated by a "D"; lines that are approximately Gaussian in the core but with indication emission extending to velocities significantly greater than twice the FWHM are indicated by a "W" (wings). The

TABLE 4

CO Line Observations of Cirrus Point Sources

| | $^{12}$CO(1–0) | | | $^{13}$CO(1–0) | | | |
|---|---|---|---|---|---|---|---|
| Name | $T_R^*$ (K) | $V_{LSR}$ (km s$^{-1}$) | FWHM[a] (km s$^{-1}$) | $T_R^*$ (K) | $V_{LSR}$ (km s$^{-1}$) | FWHM[a] (km s$^{-1}$) | Telescope and Year |
| 2716..... | 11.2 | 9.7 | 0.8 | 1.0 | 9.7 | 0.8 | HCRO 90 |
| | 7.4 | 1.2 | 1.1 | 1.2 | 9.6 | 1.1 | HCRO 90 |
| 2983..... | 11.2: | −4.2 | 1.8C | <0.6 | ... | ... | HCRO 90 |
| 4055..... | 5.4 | 11.8 | 1.3 | 1.6 | 11.9 | 0.8 | NRAO 88, FCRAO 91 |
| 4528..... | 6.9 | 4.5 | 0.7 | 1.3 | 4.6 | 0.5 | NRAO 89 MAP |
| 4642..... | 5.0 | −3.8 | 1.2 | 1.1 | −3.6 | 0.7 | NRAO 88 |
| 4655..... | 13.0 | 8.8 | 1.1 | 7.0 | 8.9 | 0.8 | NRAO 88, HCRO 91 MAP |
| 4657..... | 8.6 | −2.2 | 1.7W | 1.8 | −2.4 | 0.8 | NRAO 88 |
| 4665..... | 15.1 | −2.4 | 0.9 | 4.7 | −2.4 | 0.6 | NRAO 88 |
| 4880..... | 11.8 | −4.2 | 1.8 | 7.2 | −4.2 | 1.8 | HCRO 90 |
| 4959..... | 11.0 | 9.0 | 1.3D | 2.6 | 9.0 | 0.9 | NRAO 89 MAP |
| 4979..... | 19.3 | 10.7 | 1.0 | 7.6 | 10.8 | 0.7 | NRAO 89 MAP |
| 4991..... | 15.8 | 2.5 | 2.0W | 2.4 | 2.5 | 2.0W | HCRO 90 |
| 5270..... | 28.4 | 10.5 | 1.3C | 13.4 | 10.5 | 1.3 | HCRO 90, FCRAO 91 |
| 5299..... | 18.4 | 10.3 | 1.6W | 10.4 | 10.3 | 1.6 | HCRO 90 |
| 5431..... | 6.4 | 2.1 | 0.6 | 2.0 | 1.6 | 0.6 | HCRO 90 |
| 5812..... | 19.6 | 11.5 | 1.6 | <0.6 | ... | ... | HCRO 90 |
| 5854..... | 16.1 | 0.9 | 0.9 | 7.3 | 1.0 | 0.6 | NRAO 89 MAP |
| | 6.2 | 8.1 | 2.4W | 0.5 | 8.2 | 1.4 | NRAO 89 MAP |
| | 5.3 | 10.7 | 2.3W | 0.9 | 10.9 | 1.5 | NRAO 89 MAP |
| 5937..... | 10.6 | 8.5 | 1.7 | <0.8 | ... | ... | HCRO 90 |
| 8116..... | 6.3 | 3.2 | 1.3D | 2.1 | 3.2 | 0.8 | NRAO 88, FCRAO 91 |
| | 2.1 | 1.3 | 1.1D | <0.2 | ... | ... | RAO 88, FCRAO 91 |
| 9383..... | 0.6 | 0.7 | 0.7 | <0.1 | ... | ... | NRAO 89 MAP |
| 9530..... | 0.8 | −2.1 | 0.8 | <0.1 | ... | ... | NRAO 88 |
| 9532..... | 0.8 | −2.3 | 1.4 | <0.1 | ... | ... | NRAO 88 |
| 10882..... | 2.9 | 2.9 | 1.2 | 0.1 | 2.9 | 1.5 | NRAO 88 |
| 10909..... | 8.9 | 0.4 | 1.3 | 0.4 | 0.5 | 1.1 | NRAO 88 |
| 11617..... | 8.6 | 0.1 | 0.7 | 2.2 | 0.2 | 0.4 | NRAO 88, FCRAO 91 |
| 12453..... | 4.2 | −24.3 | 1.0 | <0.4 | ... | ... | HCRO 90 |
| 12531..... | 4.1 | −24.7 | 1.3W | 0.3 | −24.7 | 1.2 | NRAO 88 |
| 12547..... | 12. | 4.5 | 1.5 | ... | ... | ... | NRAO 88, FCRAO 91 |
| | −3.8 | 1.9 | 1.0C | ... | ... | ... | RAO 88, FCRAO 91 |
| 12558..... | 5.8 | −24.4 | 1.5 | 0.8 | −24.6 | 1.3 | HCRO 90 |
| 12639..... | 1.4 | −23.5 | 2.2D | <0.4 | ... | ... | HCRO 90 |
| 12751..... | 3.2 | −17.9 | 2.5W | 0.6 | −24.9 | 1.5 | HCRO 90 |
| 12811..... | 4.4 | −19.7 | 2.0W | 0.4 | −19.7 | 2.2 | NRAO 88 |
| 12899..... | 4.6 | −25.1 | 1.4 | 0.6 | −24.9 | 1.5 | HCRO 90 |
| 12902..... | 2.6 | −25.1 | 3.7W | <0.4 | ... | ... | HCRO 90 |
| 12920..... | 3.8 | −25.6 | 1.9D | <0.6 | ... | ... | HCRO 90 |
| 13101..... | 3.6 | −24.6 | 1.7W | <1.2 | 0.0 | 1.7 | HCRO 90 |
| 13135..... | 1.3 | 12.2 | 1.3 | ... | ... | ... | NRAO 87, FCRAO 91 |
| 18963..... | 5.1 | −5.9 | 0.9 | 0.8 | −5.9 | 0.8 | NRAO 88 |

[a] Non-Gaussian line profiles are indicated by W = wings, D = double, C = complex.

last column indicates the telescope used and the year of the observing run (followed by a "MAP" if the CO emission was mapped).

The lack of spectral features in the "blind" reference positions—that is, negative features in the position-switched spectra—demonstrates the high statistical significance of the association between most isolated cirrus point sources and molecular clouds. Out of a total of 78 observed ON/OFF pairs, 60 had detected emission in the ON position and four had detected emission in the OFF position. All sources with emission detected in the OFF position also had emission detected in the ON position, with velocity differences of less than 6 km $s^{-1}$. Further, six sources were observed to have multiple emission lines in the ON position. We found a 77% detection rate for emission from the ON positions, and 5% detection rate for the OFF positions. The detection rate for the OFF positions and the rate of detection of extra lines from the ON position are similar. Since our OFF positions are within a degree of the ON positions, which have a high detection rate, it is probable that our OFF positions are biased toward a higher likelihood of CO detection. We conclude that the chance of finding CO emission from a random patch of sky is less than 5%, and that less than four of our ON detections are due to random chance. For comparison, Magnani, Blitz, & Mundy (1985) estimate that 0.5% of the sky is filled with CO emission at the 0.3 K level, which is consistent with our limit; Heithausen & Thaddeus (1992) estimate that less than 9% of the high-latitude sky is covered by CO emission, which is consistent with but less strict than our limit.

Where mapping information was obtained, the CO was found to be extended over more than one beam. Searching the large-scale CO maps of the Perseus and Ursa Major regions made with the 1.2 m telescope (Maddalena et al. 1986; Ungerechts & Thaddeus 1987; deVries, Heithausen, & Thaddeus 1987) at the *IRAS* positions revealed that only the brightest of our cirrus point sources (C5854) included in the survey boundaries was detected. This is consistent with the beam dilution (in the 9′ beam of the 1.2 m telescope) expected for a small cloud in the coarsely sampled survey maps. The velocities of our clouds are similar to the velocities of nearby larger-scale clouds. Thus the CO emission likely arises from small, isolated regions that are sometimes fragments of larger complexes.

## 4. DERIVED PHYSICAL PROPERTIES

### 4.1. *The Nature of the Cirrus Point Sources*

We now turn to the analysis of the properties of the majority of our sources: those with no known optical, radio or near-infrared counterpart. The basic data for the cirrus point sources are the 100 $\mu$m brightness and the CO line integral, which are plotted together in Figure 5. The 100 $\mu$m surface brightness, obtained from the total source flux and estimated solid angle from the *IRAS* one-dimensional scans (§ 2.2), is shown on the $x$-axis with error bars due primarily to the 0.5 uncertainty in the source size. Many of the infrared surface brightnesses are lower limits, because the angular size is an upper limit; these sources have a different symbol (×), and caps on the error bars are double-sized in the direction disallowed by the angular size limit. The brightness of the CO (1–0) line, as observed in a single beam centered on the infrared position, is shown on the $y$-axis, with 10% and 20% error bars due to the uncertainty in absolute calibration of the NRAO and HCRO observations, respectively. There is a general correlation between the infrared and CO surface brightness, with considerable scatter and divergence at the faint end. Since the probability of detecting CO in the "blind" survey was negligible compared to the detection rate of CO at the infrared cirrus point source positions (§ 3.3), we must interpret the features of Figure 5 as real variations in the properties of interstellar material and environment responsible for the emission.

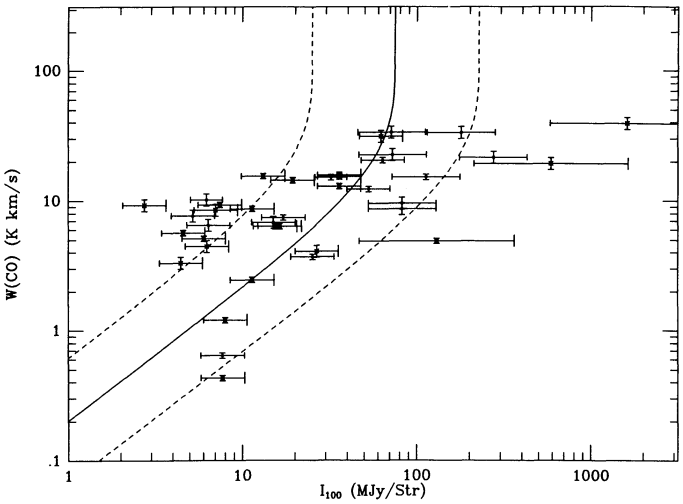


FIG. 5.—Scatter diagram of the CO (1–0) line integral and infrared surface brightness. Error bars on the infrared surface brightness are due to the uncertainty in measuring the source size, which is large because most of the sources are by definition nearly unresolved. Error bars on the CO line integral are due to uncertainty in the absolute calibration of the spectra. Both $I_{100}$ and $W$(CO) are independent of source distance if the sources are resolved. Unresolved (to *IRAS*) sources are indicated by (×), and the error bar cap is twice as large as normal in the direction allowed by the angular size limit. The solid line is the prediction of eq. (2), and the dashed lines are the predictions of the simple model if the interstellar radiation field were increased by factors of 3 (dashed curve to the right of the solid curve) and $\frac{1}{3}$ (dashed curve to the left of the solid curve).

Let us consider a simple model for a cirrus point source: the infrared emission arises from dust mixed with molecular gas in a uniform, spherical cloud; the dust is heated by the interstellar radiation field (ISRF); and its absorption cross-section is the same as that of dust in the diffuse interstellar medium. The infrared surface brightness per unit gas column density has been measured for the diffuse interstellar medium as $I_{100}/N_{\rm H} = 0.9 \pm 0.1$ MJy $sr^{-1}$ $10^{-20}$ $cm^2$, with a range of 0.5–2.1 (Tereby & Fich 1986; Boulanger & Perault 1987; deVries et al. 1987; Heiles, Reach, & Koo 1988), where $I_{100}$ is the 100 $\mu$m surface brightness and $N_{\rm H} = N_{\rm H\,I} + 2N_{\rm H_2}$ is the column density of H nuclei. (Actually, $N_{\rm H}$ is the column density of H nuclei in atoms and molecules. As of yet the infrared emission from ionized gas at high latitudes is not detected, despite its substantial column density, $N$(H II) $\sim 1 \times 10^{20}$ $cm^{-2}$ [Reynolds 1991]. The column density of ionized gas in cirrus point sources is small compared to the molecular column density, because no Hα emission is evident on the Palomar plates. We neglect H II for now, and return to it in § 4.3, where it is found to be significant for some sources.) The flux received within the solid angle subtended by a typical *IRAS* 100 $\mu$m detector (3′ × 5′) can therefore be predicted given the gas column density. If the gas is primarily molecular, and the $H_2$ column density per unit CO line integral is equal to that obtained in the Galactic plane (see Bloemen et al. 1986; Bloemen 1987), then $N_{\rm H} = 5.6 \times 10^{20} W$(CO), where $W$(CO) is the CO line integral in radioastronomical units of K km $s^{-1}$.

To take into account the fact that the radiation field inside the cloud is lower than in the diffuse ISM due to absorption in the outer layers, we shall introduce a factor $f_\tau$ such that $I_{100} = [I_{100}/N_H] f_\tau N_H$, where $[I_{100}/N_H]$ is fixed at its diffuse interstellar value. Using the radio of column density to visible extinction $N_H/A_V = 1.9 \times 10^{21}$ (Bohlin, Savage, & Drake 1987), the optical depth (at 5500 Å) from the edge to the center of the cloud is $\tau_c = W(\mathrm{CO})/7.4$. An approximation to the radiative transfer is that the central radiation field is reduced by a factor $(1 - e^{-\tau_h})/\tau_h$, where the central optical depth $\tau_h$ is evaluated at the wavelength at which the ISRF dust heating rate is maximum. Considering the shape of the ISRF (as discussed below), peak heating occurs around 8000 Å, where $\tau_h \simeq 0.5\tau_c$. (A more detailed radiative transfer model including the change in the shape of the ISRF within the cloud is given in the next section; here we derive a simple analytic approximation.)

We thus arrive at the simple relationship between the 100 $\mu$m surface brightness and the CO line integral:

$$I_{100} = 5.0\left[\frac{1 - \exp[-W(\mathrm{CO})/15]}{W(\mathrm{CO})/15}\right] W(\mathrm{CO})\ \mathrm{MJy\ sr^{-1}}\ . \quad (2)$$

This relationship is plotted as curve in Figure 5, together with two dashed curves showing the effects changing the strength of the ISRF by factors of 3 and $\frac{1}{3}$. According to the simple model, the infrared brightness is proportional to the CO line integral at low optical depths. At high optical depths, the infrared surface brightness saturates at the surface brightness of the ISRF.

Most of the cirrus point sources lie within the bounds of our simple model. There are three types of exceptional sources. (1) Sources with no CO are likely to be external galaxies with relatively high infrared surface brightness relative to the (undetected) visible brightness; this category also contains candidates for new types of astronomical object, as no counterpart at any wavelength has yet been discovered. (2) Sources with high $W(\mathrm{CO})$ and low $I_{100}$ are likely to be globules that are either dust-deficient or illuminated by a relatively low radiation field (examples are discussed individually below). (3) Sources with very high $I_{100}$, in excess of the surface brightness of the ISRF, must be heated by a locally enhanced radiation field. These sources are protostellar candidates, especially if there is short-wavelength emission from warmer dust near the protostar.

We can use equation (2) and Figure 5 to interpret cirrus point sources found in molecular clouds. If no infrared mapping information is available, then the upper limit to the angular size should be taken as $\sim 4'$, and the surface brightness calculated as $I_{100} = 0.7F_{100}$ MJy sr$^{-1}$, where $F_{100}$ is the cataloged 100 $\mu$m flux density of the source (in Jy). For example, the source IRAS 230604+145055 has been found to be strategically located within the high-latitude molecular cloud MBM 55, such that it could be interpreted as a young stellar object responsible for a low-level molecular outflow (Vallée & Avery 1990). Application of equation (2) to the CO line integral reveals that a 100 $\mu$m surface brightness of $\sim 70$ MJy sr$^{-1}$ can be expected from dust mixed with the molecular gas. The PSC flux of 2.38 Jy represents a surface brightness of greater than 2 MJy sr$^{-1}$. Thus the *IRAS* source brightness is only a small fraction of the expected dust brightness, and in this case the *IRAS* source is likely "dust in the wind". Higher angular resolution would be required to find evidence for a young stellar object. If the far-infrared flux emanates from a region smaller than 30″, or there is substantial near-infrared emission, there must be a central source heating the dust.

### 4.2. *Model for the Infrared Emission*

Let us assume again that an infrared cirrus point source is a uniform, spherical cloud, and the ISRF penetrates the cloud but is attenuated by scattering and absorption. The radiative transfer, including scattering with a Henyey-Greenstein phase function, was solved using spherical harmonics by Flannery, Roberge, & Rybicki (1980), who showed that the radiation field in the center of an interstellar cloud is substantially increased (compared to our simple model above) when multidirectional scattering is included. The mean specific intensity at optical depth $\tau$ from the surface of a cloud of central optical depth (surface to center) $\tau_c$ is

$$J_\nu(\tau) = I_\nu(0) \sum_{m=1}^{M} A_m\, i_0[k_m(\tau_c - \tau)]\ , \quad (3)$$

where $i_0(x) = \sinh x/x$. In principle, the order $M$ is infinite, but in practice only 2–5 terms are needed to obtain an excellent approximation of the exact solution. The eigenvalues $k_m$ are determined by the albedo, $\omega$, and asymmetry factor, $g$, of the medium at the appropriate frequency. The coefficients $A_m$ are determined by the central optical depth, $\tau_c$, as well as $\omega$ and $g$.

The surface brightness of the cloud is given by integrating the source function along the central line of sight through the cloud:

$$I_\nu = \int_0^{2\tau_c(\nu)} S_\nu(\tau) e^{-\tau}\, d\tau\ , \quad (4)$$

where $\tau_c(\nu)$ is the central optical depth at frequency $\nu$. For grains emitting at an equilibrium temperature, $S_\nu = B_\nu(T)$. At a given depth from the surface from the cloud, the grain temperature is determined by the heating rate,

$$\Gamma(\tau) = \int_0^\infty J_\nu(\tau)\sigma_\nu(1 - \omega) d\nu\ , \quad (5)$$

where $\sigma_\nu$ is the extinction cross section. The balance between $\Gamma(\tau)$ and the integrated emission of a grain determines its temperature. The grain absorption cross sections in the far-infrared and submillimeter regime, where the cooling occurs, are approximated by an emissivity law $\sigma_\nu \propto \nu^\alpha$, where $\alpha \simeq 1.5$. The integrated emission from such grains is proportional to $T^{4+\alpha}$. Thus the grain temperature

$$T(\tau) = T_0[\Gamma(\tau)/\Gamma_0]^{1/(4+\alpha)}\ , \quad (6)$$

where $T_0$ is the temperature of grains outside the cloud and $\Gamma_0$ is the heating rate outside the cloud, where $J_\nu = J_\nu(0)$.

The shape of the interstellar radiation field from the ultraviolet to the infrared is taken from Mathis, Mezger, & Panagia (1983, hereafter MMP). The important features of the ISRF are the total energy density and the fraction emitted at frequencies that are easily absorbed in the outer layers of the cloud. It was shown by MMP that most of the energy density of the ISRF is emitted by relatively cool stars, with spectra that peak in the near infrared; the radiation from these stars clearly dominates the heating inside clouds that are opaque to ultraviolet photons. The total intensity of the ISRF is $2.2 \times 10^{-2}$ ergs cm$^{-2}$ s$^{-1}$ (MMP). About 10% of the energy density of the ISRF is in the form of ultraviolet photons ($\lambda < 2000$ Å) from hot stars; most of the energy is emitted by cooler main-sequence and red giant stars.

Since the dust cross-sections are frequency-dependent, the shape of the radiation field changes within a cloud. In what follows, we will use the 5500 Å optical depth scale; thus the total visual extinction through a model cloud is related to the central optical depth (i.e., the optical depth from the edge to the center of the cloud) by $A_V = 2.171\tau_c$. The radiation field as a function of depth into the cloud is evaluated using equation (3) at each frequency. The heating rate as a function of depth is then calculated using equation (5), and the grain temperatures follow from equation (6). The surface brightness is finally calculated by integrating through the cloud, equation (4).

The temperature $T_0$ of grains outside the cloud is determined by the unattenuated ISRF. For spherical graphite and silicate grains, the temperature calculated by Mie theory is $\sim 19.7$ K (Draine & Anderson 1985). Small grains, with enthalpy less than the energy of heating photons, are heated stochastically, and their cooling radiation is characteristic of grains at temperatures much higher than that of larger grains (Leger & Puget 1984; Draine & Anderson 1985). We shall approximate the contribution from very small grains (VSG) as from a population of blackbody grains at elevated temperature. Based on the results of detailed models of Désert, Boulanger, & Puget (1990), we approximate the VSG temperature as 40 K, and the 100 $\mu$m optical depth due to VSGs is 200 times less that due to larger grains. Our two-temperature approximation was constructed to reproduce the 60 $\mu$m/100 $\mu$m color of grains in the diffuse ISM.

The results from our model calculations are shown in Figure 6, where the apparent color (*IRAS* 60 $\mu$m/100 $\mu$m ratio) and intensity (*IRAS* 100 $\mu$m surface brightness) are shown for a set of model clouds. The models are specified by their central optical depth, $\tau_c = 0.461A_V$, the strength of the ISRF, $\chi = (T_0/19.7)^{5.5}$, and the fractional optical depth due to VSGs, $f_{VSG}$. In Figure 6*a*, models with a range of $\chi$ and $\tau_c$ are shown, with $f_{VSG}$ fixed at the average value for the diffuse ISM. In Figure 6(*b*), models with a range of $f_{VSG}$ and $\tau_c$ are shown, with $\chi = 1$ fixed at the average ISRF. The general trend is that at high optical depths, the infrared surface brightness saturates and the 60 $\mu$m/100 $\mu$m color decreases, in accord with our intuition that thicker clouds have colder cores. The 60 $\mu$m/100 $\mu$m color is strongly dependent on $f_{VSG}$, and only weakly dependent on $\tau_c$. The 100 $\mu$m surface brightness per unit column density ($I_{100}/\tau_c$) depends strongly on $\chi$, and decreases with increasing $\tau_c$ for thick clouds. The effects of changing $\chi$ and $f_{VSG}$ are not quite orthogonal, because increasing the ISRF increases both the color temperature and surface brightness of the cloud. However, only small changes in the color temperature accompany moderate changes in the ISRF. Thus to first order, the 60 $\mu$m/100 $\mu$m color is an indicator of $f_{VSG}$, and the 100 $\mu$m surface brightness per H-nucleus column density is an indicator of $\chi$ (cf. Draine & Anderson 1985; Heiles et al. 1988; Désert et al. 1990). If the 60/100 color is used to determine $f_{VSG}$ and $\chi = 1$ is assumed, then the optical depth of a cloud can be determined by comparison with the models of Figure 6*b*. The column density of gas corresponding to these optical depths are used below for comparison to the CO column densities. It should be kept in mind that the inferred $H_2$ column densities are based on the assumptions that $\chi = 1$ and the dust/gas ratio is the same as in the diffuse ISM. As discussed below, some of the cirrus point sources have low dust/gas ratios, so that the inferred $H_2$ column densities for these sources are too small.

### 4.3. *Properties from the Molecular Observations*

Several methods have been used to convert CO line observations into column and volume densities of CO and $H_2$, gas temperatures, and nonthermal velocity dispersion. The correlation between CO line integral and $H_2$ column density that has been determined indirectly from gamma-ray intensity (the gamma-rays having been produced by interaction between cosmic rays and molecules) was used above to derive a simple

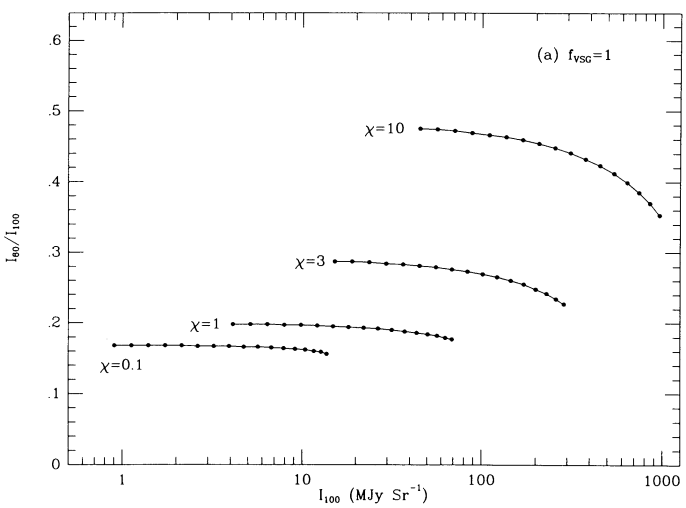


FIG. 6*a*

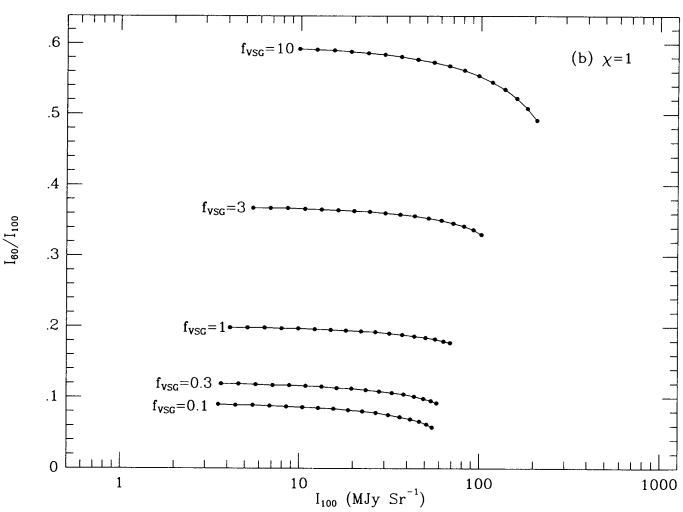


FIG. 6*b*

FIG. 6.—Far-infrared color-magnitude diagram predicted by the spherical globule model. The vertical axis is the 60 $\mu$m/100 $\mu$m brightness ratio, and the horizonal axis is the 100 $\mu$m surface brightness. Each model is specified by the central optical depth, $\tau_c$, the strength of the interstellar radiation field (relative to normal), $\chi$, and the abundance of very small grains (relative to the diffuse ISM), $f_{VSG}$. Lines are drawn to connect model predictions with fixed $\chi$ and $f_{VSG}$. The optical depth varies from $\tau_c = 0.1$ to 4, logarithmically spaced with dots at intervals $\Delta \log \tau_c = 0.1$, from the left to the right ends of the lines. (*a*) Models with "normal" abundance of very small grains, and several different interstellar radiation fields are shown. Increasing the interstellar radiation field significantly changes the surface brightness of the globule, and it also increases the 60 $\mu$m/100 $\mu$m color. (*b*) Models with normal interstellar radiation field, and several different VSG abundances are shown. Increasing the VSG abundance significantly increases the 60 $\mu$m/100 $\mu$m color, but has relatively little effect on the 100 $\mu$m surface brightness of the globule.

relationship, equation (2), between the infrared suface brightness and CO line integral. A direct relation between CO and $H_2$ is based on several assumptions that are difficult to justify. In particular, the abundance of CO, the excitation of its rotational levels, and the radiative transfer of the line photons must be the same in order for the empirical CO to $H_2$ ratio—derived primarily from low-latitude, giant molecular clouds—to apply to our high-latitude, small molecular clouds. In this section we use two different methods to analyze the CO observations.

If the excitation of the rotational levels of CO is in local thermodynamic equilibrium (LTE), and the CO and $^{13}$CO rotational levels are excited similarly, then the column density of CO may be determined analytically. In this case,

$$\frac{T_B(\mathrm{CO})}{T_B(^{13}\mathrm{CO})} = \frac{1 - e^{-\tau}}{1 - e^{-\tau_{13}}} \quad (7)$$

where $\tau$ is the optical depth of the CO line at line center, and $\tau_{13}$ is the optical depth of the $^{13}$CO line at line center. The isotope ratio of $[^{12}\mathrm{C}/^{13}] \simeq 40$–$70$ in the interstellar medium (Hawkins, Jura, & Meyer 1985; Wannier, Penzias, & Jenkins 1982; van Dishoeck & Black 1988) we will use $[\mathrm{CO}/^{13}\mathrm{CO}] = 50$ in our analysis. The observed line ratios are $\sim$2–10, implying that the CO line is thick while the $^{13}$CO line has optical depth of order unity. The excitation temperature of the (1–0) rotational transition can therefore be derived from the observed CO brightness temperature at line center, since

$$T_B = (T_{\mathrm{ex}} - T_{\mathrm{bg}})(1 - e^{-\tau}) , \quad (8)$$

where $T_{\mathrm{bg}}$ and $T_{\mathrm{ex}}$ are equal to $\lambda^2/2k$ times the Planck function evaluated at temperatures 2.74 K (cosmic background radiation) and $T_x$ (excitation temperatures), respectively. The column density of $^{13}$CO can thence be determined from

$$N^*(^{13}\mathrm{CO}) = 3.0 \times 10^{14} \frac{T_x \tau_{13}}{1 - \exp(-T_x/5.29)} \ \mathrm{cm}^{-2} , \quad (9)$$

where the $N^*$ notation is used to distinguish that the column density has been derived on the assumption of LTE (Dickman 1978). The LTE-derived excitation temperatures and CO column densities are given, for sources with $^{13}$CO observations, in Table 5.

TABLE 5

DERIVED PHYSICAL PROPERTIES

| | INFRARED GLOBULE | | | | LVG | | LTE | | | |
|---|---|---|---|---|---|---|---|---|---|---|
| NAME | $n_{H_2}$ | $\tau_c$ | $f_{VSG}$ | $\chi$ | $T_k$ | $N_{CO}$ | $T_x$ | $N^*_{CO}$ | $[CO/H_2]^a$ | $[D/G]^a$ |
| 2716..... | 4.5 | 3.2 | 0.6 | 1.3 | 19 | 16.7 | 15 | 16.8 | (−3.5) | +1.6[b] |
| 2716..... | 4.5 | 3.2 | 0.6 | 1.3 | 14 | 16.7 | 11 | 16.9 | (−3.5) | +1.6[b] |
| 2983..... | 5.0 | 3.0 | 1.0 | 3.4 | 20 | <16.5 | 16 | <16.6 | (−3.5) | +1.8 |
| 4055..... | 3.6 | 0.6 | 0.2 | 1.0 | 13 | 17.0 | 9 | 17.0 | −4.0 | (0.0) |
| 4528..... | >3.0 | 0.2 | 2.2 | 0.6 | 14 | 16.8 | 11 | 16.9 | −3.7 | (0.0) |
| 4642..... | >3.1 | 0.5 | 2.2 | 0.6 | 12 | 16.8 | 12 | 17.1 | (−5.2) | +0.8 |
| 4655..... | 3.8 | 1.0 | 1.1 | 1.0 | 17 | 17.7 | 19 | 17.6 | −3.5 | (0.0) |
| 4657..... | >4.2 | 0.4 | 0.4 | 1.0 | 16 | 16.9 | 12 | 17.1 | −4.7 | (0.0) |
| 4665..... | >4.2 | 0.7 | 0.4 | 1.0 | 23 | 17.5 | 19 | 17.6 | (−4.7) | +1.1 |
| 4880..... | 4.5 | 2.5 | 2.1 | 1.0 | 19 | 17.8 | 15 | 17.9 | −3.9 | (0.0) |
| 4959..... | 4.6 | 4.3 | 1.1 | 1.4 | 19 | 17.2 | 14 | 17.3 | (−3.5) | +1.2 |
| 4979..... | 4.3 | 2.3 | 2.1 | 1.0 | 26 | 17.7 | 23 | 17.9 | −4.0 | (0.0) |
| 4991..... | 4.5 | 3.0 | 3.5 | 0.8 | 24 | 17.2 | 19 | 17.3 | (−3.5) | +1.1 |
| 5270..... | >6.0 | ... | ... | ... | 31 | 18.0 | 32 | 18.3 | (−3.5 | +1.7 |
| 5299..... | >4.7 | 2.1 | 1.0 | 1.2 | 22 | 18.0 | 22 | 18.1 | −3.6 | (0.0) |
| 5431..... | 4.5 | 0.9 | 0.8 | 0.9 | 14 | 17.0 | 10 | 17.1 | −4.3 | (0.0) |
| 5812..... | 4.9 | 5.0 | 1.0 | 1.8 | 32 | <16.5 | 36 | <16.9 | (−3.5) | +2.0 |
| 5854..... | 4.2 | 1.3 | 0.6 | 1.0 | 23 | 17.7 | 20 | 17.9 | −3.7 | (0.0) |
| 5854..... | 4.2 | 1.3 | 0.6 | 1.0 | 14 | 16.4 | 10 | 16.5 | (−3.7) | +1.3[b] |
| 5854..... | 4.2 | 1.3 | 0.6 | 1.0 | 13 | 16.7 | 10 | 16.7 | (−3.7) | +1.0[b] |
| 5937..... | >5.6 | 5.0 | 1.0 | 3.0 | 19 | <16.7 | 14 | <16.7 | (−3.5) | +1.8 |
| 8116..... | >3.3 | 0.4 | 0.0 | 0.9 | 14 | 17.0 | 10 | 17.1 | −3.9 | (0.0) |
| 8116..... | >3.3 | 0.4 | 0.0 | 0.9 | 10 | <16.2 | 5 | <16.1 | (−3.9) | +0.8[b] |
| 9383..... | >3.2 | 0.2 | 0.4 | 0.9 | 8 | <16.5 | 4 | <16.0 | −4.2 | (0.0) |
| 9530..... | 3.2 | 0.3 | 0.9 | 0.8 | 8 | <16.3 | 4 | <16.0 | −4.5 | (0.0) |
| 9532..... | >3.2 | 0.3 | 1.1 | 0.8 | 8 | <16.2 | 4 | <15.8 | −4.4 | (0.0) |
| 10882..... | 3.7 | 0.8 | 1.7 | 0.8 | 13 | 15.7 | 7 | 15.8 | (−4.1) | +1.4 |
| 10909..... | 4.0 | 2.1 | 0.1 | 1.0 | 18 | 16.2 | 14 | 16.4 | (−3.7) | +1.7 |
| 11617..... | >4.0 | 0.6 | 0.1 | 1.0 | 16 | 17.0 | 12 | 17.2 | −4.5 | (0.0) |
| 12453..... | >3.2 | 0.2 | 0.3 | 0.9 | 12 | <16.3 | 8 | <16.3 | −4.2 | (0.0) |
| 12531..... | >3.0 | 0.2 | 0.3 | 0.9 | 14 | 16.4 | 7 | 16.2 | (−6.8) | −2.7 |
| 12558..... | >2.8 | 0.1 | 0.2 | 0.9 | 13 | 16.7 | 9 | 16.7 | (−7.) | −3.4 |
| 12639..... | >3.0 | 0.2 | 0.3 | 0.9 | 9 | <17.0 | 5 | <16.5 | (−6.8) | −3.3 |
| 12751..... | >3.2 | 0.2 | 0.4 | 0.9 | 11 | 16.7 | 6 | 16.6 | (−6.0) | −2.0 |
| 12811..... | >3.2 | 0.3 | 0.1 | 0.8 | 15 | 16.4 | 8 | 16.3 | (−5.8) | −1.4 |
| 12899..... | 3.5 | 0.5 | 0.1 | 1.0 | 13 | 16.5 | 8 | 16.5 | −4.5 | (0.0) |
| 12902..... | 3.0 | 0.2 | 0.2 | 0.9 | 10 | <16.7 | 6 | <16.4 | (−6.5) | −2.5 |
| 12920..... | 3.0 | 0.2 | 1.2 | 0.7 | 11 | <16.7 | 7 | <16.5 | (−6.5 | −2.6 |
| 13101..... | 3.1 | 0.2 | 0.2 | 0.9 | 11 | <17.1 | 7 | <16.9 | (−6.3) | −2.9 |
| 18963..... | >4.9 | 4.5 | 0.9 | 1.6 | 12 | 16.5 | 8 | 16.7 | (−3.5) | +2.0 |

[a] $[CO/H_2]$ and [D/G] are logarithms of the $CO/H_2$ and dust-to-gas ratios. The quantity in parentheses was *assumed* in order to derive the other (see § 4.4). [D/G] = 0 is a "normal" dust-to-gas ratio.

[b] Multiple CO lines detected (may not be related to *IRAS* source).

A more self-consistent method for interpreting millimeter-line observations is the large-velocity-gradient (LVG) method. If the bulk motions of the gas—which are known to exist because the linewidths are much greater than thermal—are assumed to form a large-scale gradient across the emitting region, then the coupled equations of radiative transfer and level excitation may be solved by including the escape probability in the radiative transition rates. The gas kinetic temperature and CO column density may be derived from observations of the CO and $^{13}$CO line brightnesses and line widths, but only an approximate lower limit may be set on the volume density of $H_2$. The infrared surface brightness and angular size provide an estimate of the $H_2$ volume density, typically $\sim 10^4$ cm$^{-3}$. The excitation of CO rotational levels for small molecular clouds is not very sensitive to the volume density as long as it is larger than $\sim 10^3$ cm$^{-3}$. We used the infrared estimate of the volume density in our LVG level population calculations. The LVG-derived gas temperature and CO column density are shown in Table 5.

Comparison of the LVG and LTE results reveals little difference. The gas kinetic temperature (LVG) is only slightly higher than the LTE-derived excitation temperature because collisional deexcitation dominates radiative deexcitation. Thus we have confidence that the lower limits to the volume density are not a major source of uncertainty in our analysis: at higher densities, the level populations approach LTE. The weakest assumption implicit in the LVG analysis is that the emitting region is uniform, violating our theoretical expectations that (1) the CO and $^{13}$CO are not cospatial (cf. van Dishoeck & Black 1988), (2) the $H_2$ volume density increases toward the center of the cloud (if the cloud is gravitationally bound), and (3) the gas temperature decreases toward the center of the cloud (since photoelectron emission from grains decreases dramatically where the ultraviolet part of the ISRF has been absorbed). Nonetheless the LVG method is probably the most rigorous method that can be justifiably used to interpret molecular line observations without knowledge of the structure of the emitting region.

The abundance of CO was derived using the LVG model for the CO lines and the dust cloud model for the *IRAS* fluxes. Unresolved sources have only lower limits to the $H_2$ column density, and therefore we can only derive upper limits to $[CO/H_2]$. Sources with undetected $^{13}$CO lines have only upper limits to the CO column density, so again for these sources we can only derive upper limits to the CO abundance. The derived CO abundances span the range $-3.5 > \log [CO/H_2] > -5.5$. However, many of the derived CO abundances are highly anomalous. Some optically thin cirrus clouds have high apparent CO abundances, and some optically thick cirrus clouds have low apparent CO abundances. The cosmic C abundance is an absolute upper limit to the CO abundance, barring elemental enhancements in certain regions of the ISM. If all interstellar C is in the form of CO (and none depleted into grain mantles), then $\log [CO/H_2] = -3.1$, and if depletion of C onto grain mantles is $\delta_C \simeq 0.6$, then $\log [CO/H_2] = -3.5$ (cf. Spitzer 1978). The CO abundance in translucent clouds has been theoretically predicted, including the effects of self-shielding of CO molecules from the radiation field and depth-dependent chemistry, by van Dishoeck & Black (1988). Their model $H_2$ column densities and predicted $[CO/H_2]$ abundances span the same range as our measurements, although our clouds are physically smaller and more dense than their models; also, plane-parallel geometry was used for their models, while we assume spherical geometry. The dependence of $[CO/H_2]$ on optical depth predicted by their models is not apparent in our derived properties of the cirrus point sources. Whereas low column density sources should have very low CO abundances, we find CO to be highly abundant for some sources with column densities of only $N_{H_2} \simeq 4 \times 10^{21}$ cm$^{-2}$. Conversely, whereas the CO abundance should be near its maximum value for clouds with extinction $A_V > 5$ mag, the derived CO abundance was sometimes quite low.

We are thus led to the conclusion that our assumption of constant dust-to-gas ratio is not correct. There are at least two possible explanations, both of which could be important for our sources. (1) If some of the gas is *ionized*, and there is infrared emission associated with the ionized gas, then our $H_2$ column densities (derived from the infrared brightness) are overestimated. The apparent CO abundance will therefore be small, because CO is only expected to be mixed with the $H_2$, not with the H II. Thus if an optically thick source is found to have low apparent CO abundance, we infer that there is substantial H II. (2) If the dust-to-gas ratio is lower than average, then our $H_2$ column densities (inferred from the infrared brightness) are underestimates.

### 4.4. *Sources with* H II *or Low Dust-Gas Ratio*

In Table 5 we have attempted to separate the effects of low dust-to-gas ratio and presence of H II. First, the CO abundance was calculated using the $H_2$ column density derived from the infrared brightness (§ 4.2) and the CO abundance derived from the molecular-line analysis (§ 4.3). These abundances were compared to theoretical models (van Dishoeck & Black 1988). Those sources agreeing the theoretical expectation within a factor of 3 were considered "normal," and the derived CO abundance considered real (16 sources). The rest were deemed anomalous. The difference between the $\log_{10}$ of our naively derived CO abundance and the theoretically predicted CO abundance is listed in the final column of Table 5. Positive values in this column indicate the presence of H II (11 sources), and negative values indicate a low dust-to-gas ratio (eight sources). Sources with multiple CO lines have multiple entries in the table. We can now identify which CO line is likely to be associated with the *IRAS* source: for C5854, the brightest CO line ($V_{LSR} = 1.0$ km s$^{-1}$) agrees with the *IRAS* flux with no H II or high dust-to-gas; for C8116, the brighter CO line ($V_{LSR} = 3.2$ km s$^{-1}$) agrees with the *IRAS* flux; for C2716, both components are equally likely.

#### 4.4.1. *Cirrus Point Sources That Are* H II *Regions*

Of the 11 sources with infrared excess relative to the molecular column density, five have corroborating evidence for the presence of H II. Four (C4642, C4665, C4991, C18963) were detected by us in 1400 MHz continuum with the VLA (Table 2). One (C2983) is near the California nebula, and 1400 MHz emission is evident in the Green Bank all-sky survey (Condon & Broderick 1986); our VLA map was ruined by the extended filamentary structure of the nebula. The 60 $\mu$m/100 $\mu$m $\simeq 0.33$ for C4642 and C4991 are clearly higher than the average (0.2) for sources in our sample, indicating the presence of an internal source heating the dust. For those sources with detected 1400 MHz flux, we may derive the number of recombinations per unit time and thence the rate of ionizing photons:

$$N_i \simeq 6 \times 10^{44} F_{1.4} T_4^{-0.15} d_{100}^2 \text{ s}^{-1}, \quad (10)$$

where $F_{1.4}$ is the 1400 MHz flux (in Jy), $T_4$ is the electron

temperature (in units of $10^4$ K), and $d_{100}$ is the distance to the source (in units of 100 pc). This may be compared to the ionization rate from a main-sequence star, which we approximate as a blackbody with ultraviolet color temperature $T_{\rm eff}$ and radius $R$:

$$N_i(\mathrm{MS}) \sim 10^{47} \exp(-1.4 \times 10^5/T_{\rm eff})(R/R_\odot)^2 . \quad (11)$$

The ionization rates for our sources correspond to stellar types A0–B8. If the source ionization were actually such a star, its apparent visual magnitude would be

$$m_V \simeq 5 + 5 \log d_{100} + A_V/2 .$$

Three of the detected sources may be in the Orion spur and could have distances $\sim$500 pc, suggesting $m_V \sim 10$, bright enough to be evident on the Palomar Observatory Sky Survey. The dust would be heated primarily by direct absorption of stellar radiation, with a small heating from Ly$\alpha$ photons in the recombining region. The infrared emission would be produced by a dust cloud with optical depth

$$\tau \sim 3 \times 10^{-3}(F_{100} + 2.6F_{60})(L_*/L_\odot) ,$$

where $F_{100}$ and $F_{60}$ are the *IRAS* fluxes in Jy. If the ionizing source is really an A0–B8 star, then the column density of H nuclei is $N_{\rm H} \sim 1 \times 10^{19}$ cm$^{-2}$ (using fluxes typical for the VLA-detected sources). The electron column density implied by the radio continuum observations is $N_e \sim 2 \times 10^{21} n_e^{-1} \theta^{-2}$ cm$^{-2}$, where $\theta$ is the source size in arcmin and $n_e$ is the electron volume density in cm$^{-3}$. The electron and proton column densities are equal if $n_e \sim 200\theta^{-2} d_{100}^{-2}$ cm$^{-3}$. The mass of the H II region is not large, $\sim 4 \times 10^{-4} \theta d_{100}\ M_\odot$, and could be produced by very slow mass loss from the star. At visible wavelengths, the region should be visible both as reflection nebulosity and H$\alpha$ emission ($I_{\rm H_\alpha} \sim 20$ R).

If the source of ionization for the cirrus point sources with radio continuum emission were an early-type star, then we would expect to detect evidence at visible wavelengths for the exciting star. Neither the star, nor the reflection nebulosity, nor the H$\alpha$ emission are evident within a few arcmin of the source on the Palomar Observatory Sky Survey prints. These sources are likely to be ionized by a non-main-sequence star. If the ultraviolet spectrum increases steeply with frequency, the luminosity of ionizing photons is $\sim 10^{-2}\ L_\odot$ for our sources. These sources are candidates for future observational work to determine whether they are protostars.

#### 4.4.2. *Cirrus Point Sources with Low Dust Abundance*

All of the sources with low dust-to-gas ratios are in or near the Draco nebula, a region with intermediate-velocity molecular gas and high-velocity atomic gas. It has been suggested that a high-velocity cloud is colliding into the Draco molecular cloud from the Galactic halo (Goerigk et al. 1983; Mebold et al. 1985). This distance has recently been estimated as 200–300 pc (Penprase 1992), in contrast to previous claims that the region is more than 300 pc distant (Lilienthal et al. 1991) High-velocity clouds are known to lack infrared emission, and we infer that their dust abundances are relatively low (Wakker & Boulanger 1986). We note that the CO in Draco is at an anomalous velocity ($-25$ km s$^{-1}$), in between that of typical low-velocity gas and that of the high-velocity H I ($-140$ km s$^{-1}$) in Draco. The low dust abundances we observe suggest that the molecular gas formed from dust-deficient high-velocity-cloud material. Alternatively, the dust associated with the molecular cloud could have been destroyed in a collision between the high-velocity cloud and the molecular cloud; however, it is difficult for the large dust grains to be destroyed while the CO survives. Another alternative is that the dust and gas have been displaced from one another, such as has been reported for filaments in the expanding shell in Eridanus (Veschuur et al. 1992).

### 4.5. *Unidentified Sources with No CO*

While the bulk of the cirrus point sources are associated with interstellar matter, there remain a large number that still have no identification with any other astrophysical phenomenon. In Table 6 we list the 12 sources that were observed, but not detected, in CO observations. Based on our few deep optical images of cirrus point sources (Heiles et al. 1987), we expect that many of these are simply uncataloged galaxies with higher than average infrared emission per unit optical emission. It remains to be seen if some of these are new types of astronomical object.

## 5. DISCUSSION

### 5.1. *Gravitational Binding of the Cirrus Point Sources*

The majority (70%) of infrared cirrus point sources, selected to have the highest probability of being a new class of astronomical object, were found to be molecular structures in the interstellar medium. These structures are in regions of low H I column density—so low that the column density required for $H_2$ self-shielding is exceeded only over a small volume. The existence of isolated, dense globules at high latitudes is surprising. Indeed the internal gas pressure implied by the volume density and velocity dispersion exceeds the average interstellar pressure ($p/k \sim 10^4$ cm$^{-3}$ K) by one to two orders of magnitude for most sources. This argument is not strongly dependent on the distance to the sources; in order for the implied gas pressure to be equal to the average interstellar pressure, the sources would have to be located well outside the Galaxy ($\sim$10 kpc). In fact, the pressure in intergalactic space is likely to be far smaller than the pressure in the local interstellar medium, so the clouds must be located at distances greater than 10 kpc, and have masses greater than $10^3\ M_\odot$, to be gravitationally bound. Such large distances seem unlikely because the observed velocities of the CO lines relative to the local standard of rest are small compared to Galactic differential rotation (which applies if the clouds rotate with the Galactic disk) and galaxian peculiar velocities and Hubble flow (which apply if the clouds are not bound to our Galaxy). Further, the intergalactic radiation field is likely to be smaller than the inter-

TABLE 6

UNIDENTIFIED CIRRUS POINT SOURCES WITH NO CO

| Name | R.A. (1950) | Decl. (1950) | $F_{100}$ (Jy) | $F_{60}$ (Jy) | $T_R^*$(CO) (K) |
|---|---|---|---|---|---|
| C04573..... | 05$^h$00$^m$24$^s$.0 | −08°22′52″ | 6.05 | 0.88 | 0.2> |
| C08249..... | 09 47 27.7 | +71 09 13 | 3.06 | 0.40 | 0.6> |
| C08832..... | 11 26 42.2 | +63 53 22 | 2.21 | 0.40 | 0.6> |
| C08846..... | 11 29 31.3 | +64 16 54 | 2.26 | 0.40 | 0.6> |
| C08954..... | 11 48 35.9 | +58 55 55 | 2.37 | 0.40 | 0.6> |
| C09357..... | 12 54 43.7 | +09 05 04 | 2.00 | 0.40 | 0.1> |
| C09605..... | 13 36 42.5 | +67 04 05 | 2.23 | 0.40 | 0.2> |
| C11119..... | 15 48 32.2 | −25 45 36 | 15.16 | 2.84 | 0.2> |
| C11960..... | 16 23 1.8 | −15 53 60 | 19.31 | 1.95 | 0.2> |
| C12254..... | 16 33 56.6 | +61 35 41 | 2.56 | 0.40 | 0.2> |
| C18755..... | 22 26 46.5 | −21 02 14 | 11.96 | 1.64 | 0.2> |
| C18759..... | 22 27 7.3 | −21 02 59 | 11.63 | 1.12 | 0.2> |

stellar radiation field, so it is difficult to imagine a heating source strong enough ($>10^3\ L_\odot$) to power the observed infrared emission. Thus, we conclude that the sources are located at distances that typify interstellar clouds at high latitudes, that is, less than a few hundred parsec. This means that neither are they pressure confined by the surrounding interstellar gas, nor are they gravitationally confined by their measured molecular mass.

Now consider alternative sources of mass that could gravitationally confine the sources. Those few sources with evidence for H II are likely to be gravitationally bound to the source of ionization, which could be a non-main-sequence star or protostar. The remainder of the sources are either gravitationally bound by an undetected central mass, or they are transient. The virial mass of the clouds, that is, that mass which would be sufficient for gravitational binding, is typically two orders of magnitude larger than the detected mass (i.e., the mass of dust traced by the 100 $\mu$m surface brightness and gas traced by the CO column density). Only the Draco clumps, for which we infer that the dust-to-gas mass ratio is some two orders of magnitude lower than in the diffuse ISM, are gravitationally bound by the detected gas and dust.

For those objects with insufficient gas for gravitational binding, the missing mass could be supplied by a central object with $M \simeq 6\theta(\delta v)^2 d_{100}\ M_\odot$, where $\theta \sim 3$ is the clump angular size (arcmin) and $\delta v \sim 1$ is the observed line width (km s$^{-1}$). The central object must not be a strong source of ionizing photons (lest it produce an H II region with free-free and recombination line emission), nor can it be very luminous at visible wavelengths (lest it be visible on the Palomar Sky Survey), nor can it be very luminous bolometrically (lest it heat the dust substantially above its temperature in the diffuse interstellar medium).

### 5.2. *Dead-Star Hypothesis for the Missing Mass*

One possibility for the nature of a central object that could bind the cirrus clumps is stellar remnants. If the clumps are $\gtrsim 20$ pc from the Sun, the mass required for gravitational binding is $\gtrsim 3\ M_\odot$, in which case the stellar remnant is predicted to be a black hole (cf. Shapiro & Teukolsky 1983). If the distance, angular size, or velocity dispersion of the cirrus clump are smaller than estimated above, then a less massive stellar remnant, namely a neutron star or white dwarf, could be implicated. Stellar remnants travel through the interstellar medium, accreting material at a rate that depends on the relative speed of the remnant and the column density of the medium. The accretion of interstellar matter onto old neutron stars has been addressed before (Ostriker, Rees, & Silk 1976), and it has been concluded that old neutron stars may be detectable as soft X-ray sources using the *ROSAT* survey (Treves & Colpi 1991). Using conservative estimates of the density of stellar remnants, the encounter rates, and the accretion physics, we have found that the predicted number of accretion nebulae is small (Reach, Heiles, & Koo 1993). Thus in order for the dead star hypothesis to explain the observed number of cirrus point sources, we require that one or more of our assumptions was incorrect.

## 6. SUMMARY AND FUTURE PROSPECTS

We have identified a sample of small interstellar condensations that are not associated with larger clouds. The sample was selected from the *IRAS* PSC based on their low color temperature, then further restricted based on the column density of H I in the surrounding medium. We surveyed the sources for 20 cm and 3 mm radio continuum emission, small H I clumps, and CO emission. Based on the high detection rate of CO (77%) at the *IRAS* source positions, compared to the low detection rate of CO (5%) at nearby reference positions, we conclude that most of the sources are condensations of largely molecular interstellar medium.

Some of the condensations have wide CO lines, or radio continuum emission, or both. These condensations occur primarily at the edge of the Orion-Taurus-Perseus region, and have velocities similar to nearby star-forming regions. There may be an incipient stellar condensation in the center of these clumps, with sufficient mass to gravitationally bind them. The central object could potentially be revealed by observations at high angular resolution searching for dense molecular gas or near-infrared emission from a protostellar disk. Submillimeter or far-infrared observations (at $<1'$ resolution) could provide indirect evidence for the existence of a heating source, if the surface brightness of the emission exceeds that of the interstellar radiation field.

Some of the condensations are apparently deficient in dust by two orders of magnitude, relative to the amount of molecular gas. These condensations occur only in the Draco region, where a high-velocity cloud is interacting with the lower-velocity gas. There is no need for a central object to bind these clumps, because the molecular gas mass is sufficient.

Many of the condensations have narrow CO lines, normal dust-to-gas ratios, no evidence for local dust heating above that due to the interstellar radiation field, and are apparently not associated with other interstellar complexes. These clumps are apparently far from pressure equilibrium with the diffuse interstellar medium, and thus are likely to be either transient or bound by self-gravity. Since there is little evidence for a shock that could have formed a transient density perturbation, it is likely that the objects are either hydrodynamic (or magneto-hydrodynamic) instabilities, or that they are gravitationally bound. One possibility is that these clumps could be material accreted by stellar remnants.

Many people were involved in the 11 observing and data analysis runs, including staff members at IPAC (Pasadena), NAIC (Arecibo), and NRAO (both the Tucson and Socorro branches). The VLA data were obtained remotely and calibrated by NRAO staff. W. T. R. thanks D. Levine for assistance with the *IRAS* FSDB; P. Jewell for help with the operation and calibration of the NRAO 12 m telescope; B. M. Lewis and R. Giovanelli for help with the operation of the NAIC 305 m telescope; Y. Lee for help with operation and observing, and M. Pound for help with observing and data reduction, at the FCRAO 14 m. F. Verter is gratefully acknowledged for critical reading of the observational part of the manuscript. This paper is based on work supported in part by the National Science Foundation under grant AST-8818544, and in part by a NASA (Astrophysics Data Program) grant to C. H. W. T. R. acknowledges support from an National Research Council-NASA Goddard Space Flight Center Resident Research Associateship during preparation of the manuscript.

REFERENCES


Bloemen, J. B. G. M. 1987, in Interstellar Processes, ed. D. J. Hollenbach & H. A. Thronson, Jr. (Boston: Reidel), 143
Bloeman, J. B. G. M., et al. 1986, A&A, 154, 25
Bohlin, R. C., Savage, B. D., & Drake, J. F. 1978, ApJ, 224, 132
Boulanger, F., & Perault, M. 1987, ApJ, 330, 964
Casoli, F., Dupraz, C., Gerin, M., Combes, F., & Boulanger, F. 1986, A&A, 169, 281
Cleary, M. N., Heiles, C., & Haslam, C. G. T. 1979, A&AS, 36, 95
Clemens, D. P., & Barvainis, R. 1988, ApJS, 68, 257
Condon, J. J. 1984, ApJ, 287, 461
Condon, J. J., & Broderick, J. J. 1986, AJ, 91, 1051
Crutcher, R. M. 1979, ApJ, 234, 881
Désert, F. X., Boulanger, F., & Puget, J. L. 1990, A&A, 327, 215
deVries, H. W., Heithausen, A., & Thaddeus, P. 1987, ApJ, 319, 723
Dickman, R. 1978, ApJS, 37, 407
Draine, B. T., & Anderson, N. 1985, ApJ, 292, 494
Flannery, B. P., Roberge, W., & Rybicki, G. B. 1980, ApJ, 236, 598
Goerigk, W., Mebold, U., Reif, K., Kalberla, P. M. W., & Velden, L. 1983, A&A, 120, 63
Hawkins, I., Jura, M., & Meyer, D. M. 1985, ApJ, 294, L131
Heiles, C. 1984, ApJS, 55, 585
Heiles, C., McCarthy, P. J., Reach, W. T., & Strauss, M. A. 1987, in Star Formation in Galaxies, ed. C. J. Lonsdale (NASA CP-2466), 553
Heiles, C., Reach, W. T., & Koo, B.-C. 1988, ApJ, 332, 313
Heithausen, A., & Thaddeus, P. 1992, preprint
Helou, G., Iffat, I. R., Malek, L., & Boehmer, L. 1988, ApJS, 68, 151
Houck, J. R., Schneider, D. P., Danielson, G. E., Beichman, C. A., Lonsdale, C. J., Neugebauer, G., & Soifer, B. T. 1985, ApJ, 290, L5
Infrared Processing and Analysis Center User's Guide. 1989, JPL D-2416, ed. L. Fullmer, I. Khan, G. Laughlin, D. Levine, & R. Benson (Pasadena: JPL)
*IRAS* Catalogs and Atlases: Explanatory Supplement. 1988, ed. C. A. Beichman, G. Neugebauer, H. J. Habing, P. E. Clegg, & T. J. Chester (Washington: GPO)
*IRAS* Small Scale Structure Catalog. 1988, ed. G. Helou & D. W. Walker (Washington: GPO) (SSS)
Jenker, H., Lasker, B. M., McLean, B., Russell, J., Sturch, C., & Shara, M. 1989, private communication
Jewell, P. 1988, 12 m Telescope Receiver and Calibration Status, NRAO technical memorandum
Lilienthal, D., Wennmacher, A., Herbstmeier, U., & Mebold, U. 1991, A&A, 250, 150
Maddalena, R. J., Morris, M., Moscowitz, J., & Thaddeus, P. 1986, ApJ, 303, 375
Magnani, L., Blitz, L., & Mundy, L. 1985, ApJ, 295, 402 (MBM)
Manchester, R. N., & Taylor, J. H. 1977, Pulsars (San Francisco: Freeman)
Mathis, J. S., Mezger, P. G., & Panagia, N. 1983, A&A, 128, 212 (MMP)
Mebold, U., Cernicharo, J., Velden, L., Reif, K., Crezelius, C., & Goerigk, W. 1985, A&A, 151, 427
Moshir, M., et al. 1989, Explanatory Supplement to the IRAS Faint Source Survey (Pasadena: JPL) (FSS)
Oosterbaan, C. E. 1978, A&A, 69, 235
Ostriker, J. P., Rees, M. J., & Silk, J. 1976, Ap. Lett., 6, 179
Penprase, B. E. 1992, ApJS, 83, 273
Pound, M. W., Bania, T. M., & Wilson, R. W. 1990, ApJ, 351, 165
Reach, W. T., Heiles, C., & Koo, B. C. 1988, in Interstellar Dust: Contributed Papers, ed. A. G. G. M. Tielens & L. J. Allamandola (NASA CP-3036), 309
———. 1993, in preparation
Reynolds, R. J. 1991, ApJ, 372, L19
Rice, W., Lonsdale, C. J., Soifer, B. T., Neugebauer, G., Kopan, E. L., Lloyd, L. A., de Jong, T., & Habing, H. J. 1988, ApJS, 68, 91
Shapiro, S. L., & Teukolsky, S. A. 1983, Black Holes, White Dwarfs, and Neutron Stars (New York: John Wiley)
Spitzer, L., Jr. 1978, Physical Processes in the Interstellar Medium (New York: John Wiley)
Stark, A. A., et al. 1992, ApJS, 79, 77
Tereby, S., & Fich, M. 1986, ApJ, 309, L73
Treves, A., & Colpi, M. 1991, A&A, 241, 107
Turner, B. E., Rickard, L. J., & Xu, L.-P. 1989, ApJ, 344, 292
Ulich, B. L., & Haas, R. W. 1976, ApJS, 30, 247
Ungerechts, H., & Thaddeus, P. 1987, 4, 257
Vallée, J. P., & Avery, L. W. 1990, A&A, 233, 553
van Dishoeck, E. F., & Black, J. H. 1986, ApJS, 62, 109
———. 1988, ApJ, 334, 771
Verschuur, G. L., Rickard, L. J., Verter, F., Pound, M. W., & Leisawitz, D. 1992, ApJ, 390, 514
Wakker, B. P., & Boulanger, F. 1986, A&A, 170, 84
Wannier, P. G., Penzias, A. A., & Jenkins, E. B. 1982, ApJ, 254, 100
Young, J. S., Xie, S., Kenney, J. D. P., & Rice, W. L. 1989, ApJS, 70, 699
Yun, J. L., & Clemens, D. P. 1992, ApJ, 385, L21